Ocean Sci. Discuss., doi:10.5194/os-2017-9, 2017
Manuscript under review for journal Ocean Sci.
Discussion started: 17 March 2017
© Author(s) 2017. CC-BY 3.0 License.

Ocean Science Discussions

On the deep convection events and Antarctic Bottom Water formation in ocean reanalysis products

Wilton Aguiar[1], Mauricio M. Mata[1] and Rodrigo Kerr[1]

[1]Laboratório de Estudos dos Oceanos e Clima, Instituto de Oceanografia, Universidade Federal de Rio Grande – FURG. Rio Grande, RS, 96203-900, Brazil.

Correspondence to: Wilton Aguiar (aguiar.wilton@gmail.com)

Abstract.

Deep convection in open ocean polynyas are common sources of error on the representation of Antarctic Bottom Water (AABW) formation in Ocean General Circulation Models. Even though those events are well described in non-assimilatory ocean simulations, recent appearance of open ocean polynya in Estimating the Circulation and Climate of the Ocean Phase II reanalysis product raises a question if this spurious event is also found in state-of-art reanalysis products. In order to answer this question, we evaluate how three recently released high-resolution ocean reanalysis form AABW in their simulations. We found that two of them (ECCO2 and SoSE) create AABW by open ocean deep convection events in Weddell Sea, showing that assimilation of sea ice has not been enough to avoid open ocean polynya appearance. The third reanalysis – My Ocean University Reading – actually creates AABW by a rather dynamically accurate mechanism, depicting both continental shelf convection, and exporting of *Dense Shelf Water* to open ocean. Although the accuracy of the AABW formation in this reanalysis allow an advance in represent this process, the differences found between the real ocean and the simulated one suggests that ocean reanalysis still need substantial improvements to accurately represent AABW formation.

1 Introduction

Currently, different groups of experts have developed several state-of-art eddy-permitting general ocean circulation models with longer simulations and elegant assimilation methods. Based upon those models, the reconstruction of oceanic features by governing ocean equations and observed data, named ocean reanalysis products, have been coupled with global climate models (GCMs) to produce detailed climate estimates (e.g Lee et al., 2009). Specific climate induced studies using ocean reanalysis focus on several features, such as the description of sources for Antarctic dense water mass contributions (Kerr et al. 2012a), estimates of sea level variability (Berge-Nguyen et al., 2008; Köhl and Stammer, 2008; Wunsch et al., 2007), surface circulation and heat content of specific ocean basins (Schiller et al., 2008; Zhu et al., 2012), as well as decadal variability of ocean heat content (Carton et al., 2005). One of the features receiving attention in ocean reanalysis products is

Ocean Sci. Discuss., doi:10.5194/os-2017-9, 2017
Manuscript under review for journal Ocean Sci.
Discussion started: 17 March 2017
© Author(s) 2017. CC-BY 3.0 License.

the representation of the lower limb of the Atlantic Meridional Overturning Circulation (AMOC), particularly due to the recent observed trends in the Southern Ocean bottom layer (Azaneu et al., 2013; Purkey and Johnson, 2012). In this sense, recent assessments have shown some model inconsistencies related to the Southern Ocean dense water formation and export, which is a key process to the AMOC lower limb dynamics (e.g. Azaneu et al., 2014).

The dense bottom waters in the Southern Ocean are formed mainly by two mechanisms. The first one is through (i) a complex interaction of deep and shelf waters and starts with deep waters, originally formed in the North Atlantic, being transported to the south through the AMOC, changing its properties and along the way forming *Circumpolar Deep Water* (CDW) as it enters the Southern Ocean domain (e.g. Talley, 2013). There, CDW circulates along with the Antarctic Circumpolar Current (ACC) and is eventually advected towards the Antarctic coastal margin. Near the coastal margins, the interaction of CDW-derived waters with *High Salinity Shelf Water* (HSSW) formed from brine released during winter, enhance CDW density, and creates *Antarctic Bottom Water* (AABW; Carmack and Foster, 1975; Foster and Carmack, 1976). Alternatively, HSSW can circulate under ice shelves, losing heat and salt to create *Ice Shelf Water*. *Ice Shelf Water* then flows downslope and mixes with deep waters to create AABW (Foldvik et al., 1985; Nicholls et al., 2009). The coastal AABW formation occurs especially in the Weddell Sea, which is considered one of the Southern Ocean zones of highest AABW production (e.g. Orsi et al. 1999; Kerr et al. 2012b). Other sparse regions around the Antarctic continent also contribute to bottom water formation, such as Prydz Bay in the Indian Ocean sector of the Southern Ocean (e.g. Williams et al., 2016), Adélie Land (e.g. Williams et al., 2008) and Ross Sea (e.g. Whitworth and Orsi, 2006) in the Pacific Ocean sector of the Southern Ocean.

This complex coastal formation process of bottom waters is notably difficult to represent in GCMs, and instead GCMs create AABW through an alternative mechanism of (ii) open ocean deep convection. Open ocean deep convection in Southern Ocean happens when the water column stability decreases allowing heat transference to the surface, and hence creating an ice-free region, which is by definition an open ocean polynya. In the open ocean polynya, saline deep waters lose sensible heat to the atmosphere, creating AABW by cooling (Killworth, 1983). This process rarely occurs in the real ocean. In fact, the last known large open ocean polynya event was documented by Gordon (1978) and Carsey (1980), who reported a feature with 350,000 km^2 during the winters of 1974-1976 in the Weddell Sea. Although smaller size ocean polynyas happened in the 20th century (e.g. Comiso and Gordon, 1987), no winter ice-free area has been reported in Southern Ocean, with the dimensions and persistence of the Weddell Polynya, since the 70s events.

Nevertheless, ocean simulations recurrently represent bottom water formation by spurious open ocean deep convection events. Recently, Azaneu et al. (2014) evaluated the AABW properties in the *Estimating the Circulation and Climate of the Ocean Phase II* (ECCO2) and found that an intense pulse of AABW formation happens in this reanalysis as a result of the opening of an unrealistic polynya in Weddell Sea. After the polynya opening, bottom layer transports and densities become unrealistically high, and all Southern Ocean representation turns unreliable. Moreover, Heuzé et al. (2013) found that all fifteen models of the Coupled Model Intercomparison Project (CMIP) Phase 5 fail to represent the dense waters formation accurately, creating AABW by open ocean deep convection instead. Several other simulations also reported unexpected open

Ocean Sci. Discuss., doi:10.5194/os-2017-9, 2017
Manuscript under review for journal Ocean Sci.
Discussion started: 17 March 2017
© Author(s) 2017. CC-BY 3.0 License.

ocean polynyas creating AABW (Marsland et al. 2003; Timmermann and Beckmann 2004; Shaffrey et al. 2009). The frequent occurrence of open ocean deep convection events in simulations raises a question if that unrealistic pattern is found in recently released reanalysis products, and if not, how those products represent the AABW formation issue? In this study, we analyzed three recent ocean reanalysis products, with documented evidence of AABW formation, to determine if open ocean convection is the common reason for the anomalous AABW formation in those products. Moreover, we investigate other mechanisms by which bottom water is created in each ocean reanalysis.

2 Ocean Reanalysis data sets and Methods

Three ocean reanalysis products were evaluated here. The first product investigated was ECCO2, which was chosen to be used as a comparison standard to the other reanalysis due to a deep convection event triggered by the polynya opening in Weddell Sea after 2004 (Azaneu et al. 2014). This coupled ocean reanalysis is based in the Massachusetts Institute of Technology General Circulation Model (MITgcm) with a cube-sphere grid, as described by Marshall et al. (1997). The cube-92 solution used in ECCO2 is forced by the Japanese 25-Year atmospheric Reanalysis (JRA-25). A sea ice model that estimates snow cover, sea ice thickness and concentration by Zhang et al. (1998) is incorporated in ECCO2 framework, and a Green's function method assimilates ocean variables and reduce model error, as described by Menemenlis et al. (2005). ECCO2 reanalysis product spans from 1992 until 2012, with 0.25° × 0.25° horizontal resolution and 50 vertical levels unevenly spaced (Menemenlis et al., 2008).

We chose to work with other two reanalysis products with evidence of rapid AABW formation, i.e., rapid density increase in deep and bottom waters: *Southern Ocean State Estimate version 2* (hereafter referred to as SoSE) and *My Ocean University of Reading – UR025.4* (hereafter referred to as UR025.4). The SoSE has documented wintertime deep convection during the test runs (Mazloff et al., 2010). SoSE also uses the MITgcm ocean model, but it estimates the air-sea buoyancy fluxes using NCEP-National Center for Atmospheric Research reanalysis as atmospheric forcing. The framework includes a sea ice model by Hibler (1980) and assimilation through a least square fit with observations to reduce model error. SoSE horizontal resolution is of 0.16° degrees, with 42 irregular vertical levels, and a time span from 2005 until 2010. Finally, we looked at the UR025.4 product as it exhibits increasing neutral density in both deep and bottom layers of Weddell Sea after 2004 (Dotto et al., 2014), which suggests AABW formation. UR025.4 uses NEMO version 3.2 ocean circulation model, forced by ERA-Interim Atmospheric Reanalysis, and incorporates Louvain-la-Neuve Ice model Version 2 (LIM2; Fichefet & Maqueda 1997). The Optimal Interpolation Scheme from the UK Met Office operational FOAM-NEMO system was used to assimilate ocean variables (Storkey et al., 2010). UR025.4 covers the time range from 1993 until 2010, and has a tripolar grid with mean horizontal resolution of 0.25° × 0.25°, and 75 vertical levels (Ferry et al., 2012). Those distinct patterns between the reanalysis products help to track how different features in the framework of the simulations affect AABW production.

ECCO2 and SoSE are available in National Aeronautics and Space Administration Jet Propulsion Laboratory (NASA; http://ecco2.jpl.nasa.gov/) and Scripps Institute of Oceanography (http://sose.ucsd.edu/) websites, respectively. UR025.4

© Author(s) 2017. CC-BY 3.0 License.

simulations are available in the Centre for Environmental Data Analysis of the United Kingdom web page (http://catalogue.ceda.ac.uk/uuid/ef3e53aef4dca2030ebc9e84aa908d74).

As sea ice formation and melting has direct relation to AABW formation, mean sea ice concentration and thickness have been analyzed in the present study. For a better description of distinct regional AABW formation processes and sea ice patterns, we have split the Southern Ocean into five sectors, following Parkinson & Cavalieri (2012): From 130°W until 60°W the Bellingshausen and Amundsen seas sector, from 60°W until 20°E the Weddell Sea sector, from 20°E until 90°E the Indian Ocean sector, from 90°E until 160°E the Western Pacific sector and, finally, from 160°E until 130°W the Ross Sea sector (Figure 1). Mean annual averages of sea ice concentration and thickness were compared by sectors between the reanalysis to identify the relationships between sea ice and AABW formation processes. Comparison with the observational dataset was necessary to grasp the sea ice seasonal variations veracity, and for the comparison we used the sea ice concentration product derived from Special Sensor Microwave/Imagers (SSM/I) and Special Sensor Microwave Imager/Sounder (SSMI/S) provided by National Snow and Ice Data Center (https://nsidc.org/). Both SSM/I and SSMI/S come from Nimbus-7 Scanning Multichannel Microwave Radiometer.

We analyzed oceanic regions south of 60°S and estimated the volume of water masses by sector. To achieve that, we used the water mass definitions by neutral density layers (γ^n; Jackett & McDougall 1997; Serazin 2011). The three reanalysis provide potential temperature and salinity, which were used to calculate the neutral density throughout this study. For the majority of the sectors, three water masses were defined: *Antarctic Bottom Water* (AABW), with neutral densities higher than 28.27 kg m^{-3}, *Lower Circumpolar Deep Water* (LCDW), with γ^n ranging from 28 kg m^{-3} until 28.27 kg m^{-3}, and *Upper Circumpolar Deep Water* (UCDW) with values from 27.7 kg m^{-3} until 28 kg m^{-3}, following Abernathey et al. (2016). Waters with densities lower than 27.7 kg m^{-3} were analyzed as a single group of "surface waters". As the Weddell Sea has different water mass structure (Fahrbach et al., 2004; Kerr et al., 2009a; Orsi et al., 1999), the layers were split as: *Weddell Sea Bottom Water* (WSBW) with neutral densities higher than 28.4 kg m^{-3}, *Weddell Sea Deep Water* (WSDW) between 28.27 kg m^{-3} and 28.4 kg m^{-3}, *Warm Deep Water* (WDW) from 28.1 kg m^{-3} until 28.27 kg m^{-3}, and in the shallowest end, the *Antarctic Surface Water* (AASW) with neutral densities lower than 28.1 kg m^{-3} (Naveira Garabato et al., 2002; Franco et al., 2007). The total volume of each water mass by sector was calculated by an integration described in Eq. (1):

$$V_{wm} = \frac{100}{V_{sector}} \int_{L_{coast}}^{60°S} \int_{Wl}^{EL} \int_{z_{\gamma 2}}^{z_{\gamma 1}} dz\, dx\, dy, \quad (1)$$

in which $z_{\gamma 1}$ and $z_{\gamma 2}$ are the depth of the upper and lower neutral density limit of each water mass in each cell, and dx and dy are respectively the zonal and meridional length of each cell. Although dx and dy are not constant through the reanalysis grids, the integration process takes that into account so that the water mass estimates were not contaminated by errors due to the non-uniform cell size. The result of the vertical integration is then integrated again meridionally between 60°S and the latitude of the coastline (L_{coast}), and zonally between the eastern (EL) and western (WL) limit of each section. This way, the result of equation 1 is the volume of the water mass (V_{wm}) relative to the total water volume of each sector (V_{sector}) in percentage. Those monthly volumetric percentages were then used to infer about the transformation and pulses of AABW as

© Author(s) 2017. CC-BY 3.0 License.

well as the processes involved. Finally, for a better description of the AABW formation process in UR025.4, we included the analysis of the sea ice and ocean currents velocities.

3 Results and Discussion

We will first describe the sea ice mean patterns by sector, its spatial signature and evidence that this property is related to AABW formation in the reanalysis studied (Sect. 3.1). In the next section (Sect. 3.2), we discuss the water mass volume changes in each sector to scrutinize the triggers of deep convection in the different products. Finally, in Section 3.3, we highlight the differences of the AABW formation process in the three reanalysis and the real ocean AABW formation.

3.1 Sea Ice Concentration and AABW formation pulses

As seen in Figure 2, both UR025.4 and ECCO2 overestimate the annual mean sea ice concentrations when compared to National Snow and Ice Data Center observations (hereafter referred to as NSIDC) in all sectors until 2004, except in Ross and Bellingshausen seas, where the concentrations closely follow the ones obtained from NSIDC. The sectors with the highest overestimates are the Weddell and Indian sectors, where the model cells have at least 20% more sea ice cover than observations. Previous experiments with LIM2, under the atmospheric forcing of NCEP/NCAR, show enhanced sea ice extent within the seasonal cycle, and a tendency to overestimate the sea ice thickness in Weddell Sea. The pattern of ice thickness overestimation in LIM2 was reported in the previous study to be due to westerlies stronger than real in NCEP/NCAR forcing (Massonnet et al., 2011). Although UR025.4 uses LIM2 model, a different atmospheric forcing is applied (ERA-INTERIM), and when analyzing carefully coastal wind speeds and directions, one finds no significant westerlies overestimation. Nevertheless, UR025.4 still overestimates sea ice thickness (SIT) in Weddell Sea.

The analysis performed by Azaneu et al. (2014) shows that the high annual sea ice cover of ECCO2 is due to an overestimate of maximum sea ice in winter, thus rising the annual mean. However, ECCO2 is the reanalysis that better represents sea ice concentration (SIC) before 2004. It is important to highlight that both aforementioned reanalysis exhibit interannual variability patterns close to observations. It is only after 2004 that the most noticeable spurious signals in sea ice takes place. The SIC and SIT in Weddell Sea and Indian Ocean sectors in ECCO2 decreases quickly by approximately 20%, hence lowering the whole Southern Ocean average. This decreasing pattern is unrealistic since satellite observations of NSIDC show no such alteration. Also, estimates of sea ice extent in those sectors point to an actual increase until 2010 (Parkinson & Cavalieri 2012). Hence, ECCO2 sea ice decrease points to the appearance of an open ocean polynya. Different from ECCO2, UR025.4 exhibits annual SIT increase in Weddell Sea, almost doubling that signal in 2009. Even though, to our knowledge no observational sea ice thickness database that covers efficiently the Southern Ocean is currently available, the comparison among the three reanalysis thicknesses and the magnitude of the signal suggest an UR025.4 overestimate. In spite of SoSE

Ocean Sci. Discuss., doi:10.5194/os-2017-9, 2017
Manuscript under review for journal Ocean Sci.
Discussion started: 17 March 2017
© Author(s) 2017. CC-BY 3.0 License.

sea ice concentration and thickness being available only between 2005 and 2010, their variability seems to follow observations, with mean SIC being also higher than observed. SoSE has annual mean SIT values close to ECCO2.

The anomalous signals in mean SIC and SIT in ECCO2 and SoSE reanalysis are connected to the appearance of polynyas in Weddell Sea sector, and to alterations in the mean neutral density layers. A large-scale sensible heat polynya happens in ECCO2 (Figure 1a-c). It starts to open by November 2003 near 20°E and spreads into Weddell Sea, Indian Ocean and even Ross Sea sectors, reaching the border of the sea ice, and lowering mean SIC and SIT in all Southern Ocean. At the beginning of the polynya opening process in the Weddell Sea, only WDW is found in the intermediate layer. As the ECCO2 polynya spreads, the heat loss through the surface waters increase, and so their buoyancy diminishes. Neutral densities increase at intermediate layers, forming WSDW by cooling at the prime meridian initially, and then expanding the WSDW formation to the entire Weddell Sea (Figure 1d-f). The decrease of sea ice content that contributed to the polynya opening in ECCO2 could have been caused by several factors, such as alterations on the balance of heat between the atmosphere and heat supplied by the ocean under the mixed layer (Close and Goosse, 2013), and mixing of warmer and saltier intermediate waters with surface waters (Morales-Maqueda et al., 2004). ECCO2 polynya stays open and expanding until the end of the reanalysis, creating gradually higher volume of AABW in each sector and suggesting constant heat delivery to the surface layers to maintain the sea ice melting.

SoSE reanalysis shows the presence of an open ocean polynya in the first year of simulation from May until November 2005 in Weddell Sea sector (Figure 3a). From January until May, before the polynya opening, it is noticeable in SoSE neutral density vertical distribution the presence of WDW in a very shallow depth around 70°W. WSDW and WSBW upper limits are located at approximately 1500 m and 4000 m depth, respectively (Figure 3b). After May, with the advance of the sea ice in winter, this WDW at surface cools down, but its enduring high heat content delays sea ice formation until December, allowing the open ocean polynya to form. As a result, the mean sea ice thickness in 2005 for Weddell Sea sector is the lowest of the entire SoSE time series. Neutral densities, after the polynya opening, show a shift of WSDW neutral density boundary towards the surface, increasing the total WSDW layer thickness (Figure 3c). Consequently, WDW layer thickness decreases. WDW has a higher temperature and salt content relative to local overlying AASW. The heat loss in the polynya during the winter allows WDW to lose buoyancy, forming WSDW from May until November. By December, the polynya closes and the WSDW formation slows down. WSDW formation happens also in the following two winters, but in a smaller scale.

In UR025.4 a different process occurs. After 2005, SIT in eastern Antarctic Peninsula rise, reaching values higher than three meters in 2009, and only then starting to decrease (Figure 4a-c). This persistent and regional sea ice increase is strong enough to growth mean Southern Ocean total SIT. The intense sea ice thickening signal suggests strong brine release, a process that could create AABW. The thickening signal is not seen in any other sector. Moreover, UR025.4 sea ice concentration does not show any anomalous increase elsewhere in the Southern Ocean either. Before the thickening event, only WDW is found in intermediate depths at around 700 m in the Weddell Sea . After 2007, WSDW is formed (Figure 4d-f)

Ocean Sci. Discuss., doi:10.5194/os-2017-9, 2017
Manuscript under review for journal Ocean Sci.
Discussion started: 17 March 2017
© Author(s) 2017. CC-BY 3.0 License.

by the massive sea ice formation in Weddell Sea, releasing brine continuously. WSDW production area expands from 2007 to 2010, taking all the eastern Antarctic Peninsula until the prime meridian.

Hence, the anomalous sea ice patterns in all three reanalysis should impose distinct variability to the WDW and WSDW content in Weddell Sea and Indian Ocean sectors. Further analysis of the water masses content in each model is performed to investigate this issue.

3.2 Water mass percentages by sector

Although the water mass percentages of both ECCO2 and UR025.4 reanalysis products are very similar in the beginning of their time series (Figure 5), ECCO2 exhibits the biggest shift in the percentages of water masses from the beginning of the time series until the end. AASW in this reanalysis occupies 10% of the Weddell Sea sector in 1992, and its contribution decreases throughout the time series. An initial slow decrease happens until 2000 and after that, the percentage goes down with a stronger pace reaching marks lower than 5% at the end of the series, i.e. half of its initial volume. With the decrease of the surface waters volume, seasonal cycles of AASW formation seem more apparent. While AASW percentages decline, the WDW volume seems to increase from its initial value of roughly 36%. This slow and steady increase reaches its highest value of 38% in 2000 and stays relatively stable until 2004. After that, volume percentages of WDW decay swiftly. This change leads WDW to show volume percentages lower than 10% in 2012. The initial reduction of AASW volume and increment of underlying WDW volume causes the latter water mass core to migrate progressively to shallower depths, enhancing its mixing with the surface. The WDW is warmer and saltier than AASW, so the intensive cooling of this water mass by open ocean deep convection has the potential to form WSDW and even WSBW. In fact, after 2000, when WDW reaches its highest percentage, WSDW volume starts to increase gradually, evidencing an intensification in the production. After 2004, WSDW formation is enhanced due to the polynya opening. The mechanism explaining the polynya opening is the same one thought to trigger the 70s Weddell Polynya, in which WDW rose to near surface, exchanging heat with the overlying sea ice, and allowing an ice-free area to form AABW varieties in the Weddell Sea (e.g. Killworth, 1983; Cheon et al. 2015). After 2008, it seems that with the expansion of the polynya area, heat exchange intensifies even further and WSBW starts to form in the region. During that time, WSDW formation stops and rapid conversion of WSDW to WSBW also occurs. In fact, during that period, WSBW percentage rises from 9% to unrealistic 70% of the water volume within the Weddell Sea.

SoSE reanalysis product shows similar changes to the ones reported in ECCO2. Although SoSE time series is shorter in length, it is easy to see that WDW volume for the whole series is at its highest by the beginning of 2005 (Figure 5). From May until November of 2005, the polynya in Weddell opens in SoSE, and the relatively high water volume of 32.6% of WDW swiftly decreases to 26%, and AASW decreases by its volume by 2%. During that period, WSDW percentage rises by 6%, pointing to transformation of WDW into those denser water masses during the polynya period. Moreover, WSBW is also formed in the beginning of the winter: a small increase from 14.8% to 16.6%, but in the end of the winter the WSBW

© Author(s) 2017. CC-BY 3.0 License.

volume goes back to 14.9%, thus showing no net conversion. In the following winter, the polynya does not open, but still WSDW created in 2005 keeps being converted to WSBW in the following two winters. In fact, in the winters of 2006 and 2007, the WSDW percentage decrease matches the rise in WSBW and AASW volume percentages. Just as observed in ECCO2, the process seems to initiate with a high WDW content, interacting near the surface in that region.

In UR025.4, we can see that water mass changes for Weddell Sea sector induces small amplitude oscillation of both WSDW and WSBW volume percentages (Figure 5). AASW volume in UR025.4 product, when compared with ECCO2, has more pronounced seasonality from 1994 until the winter of 2005. In the winter of 2005, a drop of 2.5% in AASW percentage happens, and in 2008 another decrease of 3% is evident, thus lowering its total volume along time. During every winter, WDW volumes drop, and WSDW and WSBW have small increases in percentage. This opposite pattern also shows a seasonal trend of conversion of AASW and WDW into WSDW and WSBW. Although the UR025.4 formation of AABW in the Weddell Sea is lower than in the previous reanalysis products, two clear pulses happen in the winter of 2008 and 2009, probably due to the salt input during the SIT increase episodes.

Differently from the other reanalysis, the biggest pulse of AABW formation in UR025.4 originates from the Indian Ocean sector. In this sector, the water masses distribution along the water column is different from the Weddell Sea, and so the analysis was carried out with the appropriate vertical layers (as explained in Sect. 2). A pulse of AABW volume percentage happens during the winter of 2004 (Figure 6) with values spanning from 43.4% to 51.8%, and during the same winter season, LCDW volume decreases by 6%. After that winter, AABW volume stays high, and LCDW remains low until the end of the reanalysis time series. That pattern suggests an event of transformation of LCDW into AABW. The 2% left of the conversion is a product of the UCDW. Actually, in May 2004 UCDW increases its volume by 3%, and afterwards further decreases its volume by 5.5%, summing a net 2.5% decrease in water mass volume. This net decrease of 2.5% complements the AABW volume increase observed in Figure 6.

Relatively high salinity and temperature CDW-derived waters, while entering the Prydz Bay surroundings in real Southern Ocean interact with ice shelves and sea ice forming *Dense Shelf Water* (DSW). The later, when exported downslope mixes with denser CDW layers and form the regional AABW variety (Williams et al., 2016). The water mass pulses seen in the Indian Ocean sector suggests that a similar process is occurring in UR025.4. UCDW is warmer and fresher than the regional LCDW that circulates along the coast. Hence, while the UCDW circulates along the sea ice edge in UR025.4, it causes melting of sea ice, lowering the surface temperature and surface salinity. Those lower salinity and temperature surface waters are then transported through the Antarctic Coastal Current westward. Moreover, their higher freezing point potentially enhance sea ice formation (and thus brine release) as they flow downstream, i.e. over LCDW waters. That process concentrates salt over the LCDW, raising its density and forming DSW by continental shelf deep convection (Figure 8). After formed, the DSW in UR025.4 flows downslope, enhancing LCDW salinity and creating a very saline variety of AABW.

The small excess of UCDW that did not interact near Prydz Bay in UR025.4 was carried through Antarctic Coastal Current until the Weddell Gyre Western border, together with the underlying high salinity LCDW, and part of the AABW formed

Ocean Sci. Discuss., doi:10.5194/os-2017-9, 2017
Manuscript under review for journal Ocean Sci.
Discussion started: 17 March 2017
© Author(s) 2017. CC-BY 3.0 License.

(observed in the model animations, not shown). This AABW advection from Indian Ocean sector is a successful representation of the process by which real ocean AABW enters Weddell Gyre (e.g. Meredith et al., 2000; Jullion et al., 2014). AABW is also formed locally in the Weddell Sea sector, due to the UCDW advection. UCDW of Indian origin is colder and has lower salinity than WDW. As a result from the process above, initially a freshening signal occurs in the Weddell Sea surface. As waters with lower salinity can boost sea ice formation, in the following winters of 2007-2009 sea ice production is enhanced in Weddell Sea, and SIT rises rapidly. The brine rejected that follows the enhanced freezing produces a HSSW pulse in the Weddell Sea, which flows down the water column, mixes with local WDW and WSDW, thus forming WSBW (Figure 4). This process occurring in the Weddell Sea seems to be responsible for the small AABW pulses observed in figure 5. The entrainment of CDW from Indian Ocean sector causing AABW formation and export in Weddell sea is a process recently suggested in real Southern Ocean (Couldrey et al., 2013), even though sea ice thickening was not reported in the study. Other factors then freshening likely contributed to the increased sea ice thickness in Weddell Sea, such as the LIM2 ice model tendency to overestimate SIT reported by Massonnet et al. (2011). However, because the atmospheric forcing used by that study is different from the one used in UR025.4, we do not believe that the overestimation trend played a major role in this simulation. In any case, validation of ERA-INTERIM wind fields have not reported overestimation of the westerlies around Antarctic Peninsula (Dee et al., 2011). Furthermore, the increased sea ice thickness in Weddell Sea could also be due to the advection of sea ice from Indian Ocean and Western Pacific sectors, as will be explained below. Different from ECCO2 and SoSE, UR025.4 does not form an open ocean polynya, and that could be because that model does not show either an increase of WDW volume reaching surface nor a diminishment of AASW volume. ECCO2 AABW volume percentages for Indian Ocean sector also result from the formation process in the Weddell Polynya (Figure 6). AABW volume rises due to WSDW and WSBW formation and advection through the ACC, and both LCDW and UCDW decrease due to local density increase after the polynya expansion to the Indian Ocean sector. Since SoSE polynya was smaller and with shorter duration than ECCO2, the AABW formation had only regional impact, not showing the AABW pulse in any other sector.

A similar process to the one occurring in UR025.4 Indian Ocean sector happens in the Western Pacific sector. An AABW pulse with 10% increase in volume happens parallel to a decrease of total 8% in both LCDW and UCDW volume in 2004 winter (Figure 7). The 2% left is converted from surface water volume. Those percentage alterations also show a conversion of CDW to AABW. However, otherwise from the Indian Ocean sector, no previous rise in UCDW volume is clear in volumetric percentages. Figure 8 shows that UCDW coming from Indian Ocean sector actually entered Western Pacific sector, even though the volume was not enough to show up in the total UCDW volume series. As UCDW enters the Western Pacific sector, it also causes sea ice melting, causing initial freshening and cooling of UCDW. In Figure 8, it is possible to notice that the ACoC strengthens after the UCDW inflow. Since in April, the area surrounding Vincennes Bay (66.5°S, 109.5°E) is covered by sea ice in UR025.4, a reasonable cause of the current intensification is the temperature/salinity gradient between UCDW and LCDW. UCDW is fresher and warmer than LCDW, inducing a density gradient directed east along the coast. As a response to that gradient, a strong current opposite to the gradient (i.e. a westward flow) appears in

© Author(s) 2017. CC-BY 3.0 License.

April contributing to speed up the ACoC near Vincennes Bay (Figure 8d). After June (Figure 8f), the intense DSW formation seems to recirculate next to Vincennes Bay and is further exported northwest also due to a strong southeast density gradient. In any case, relatively fresh UCDW from sea ice melt was transported by both the strong ACoC and the offshore-directed buoyancy current. As it is transported, UCDW loses even more heat, enhancing freezing and releasing brine over both LCDW an UCDW, and hence favoring the conditions to create DSW (Figure 8 a, c and f). Furthermore, the high density of DSW leads to deep convection next to the continental shelf, with the water flowing down the slope mixing even more with LCDW, and thus forming AABW. Hence, the higher inflow of UCDW in both Indian Ocean and Western Pacific sectors triggers a balance between melting and sea ice formation that favors LCDW salinity increase and ACoC acceleration. The fast baroclinic current that speeds up the ACoC enhances the transport of newly formed sea ice to Weddell Sea, possibly accumulating it near the Antarctic Peninsula. The enhanced sea ice advection also allows new sea ice to form, thus not accumulating at the original sector. As a result, Indian Ocean and Western Pacific sectors would have salinity increase without accountable signal of changes in mean SIC and SIT. SoSE AABW volume percentages for Western Pacific shows no pulse of AABW formation, while ECCO2 water masses for this sector shows exactly the same patterns as seen in the Indian Ocean sector, with LCDW volume rising until the polynya reach that sector (i.e. leading to form AABW locally). In fact, the ECCO2 signature of AABW production has been seen in all sectors as the polynya expands, except Bellingshausen and Amundsen seas sectors (Figures 5 - 10).

The time series of Ross Sea water masses does not show major changes due to the ECCO2 polynya mechanism until 2010 (Figure 9). In the first eighteen years of the reanalysis (1992-2010), LCDW volume percentage rises, while AABW volume percentage decreases. After 2010, with the expansion of the polynya to the Ross Sea sector in UR025.4, AABW shows a small increase in volume during the winter of 2004. Finally, no pulse of AABW is seen in any of the three reanalysis in Bellingshausen and Amundsen sector (Figure 10), which is expected since this sector in real Southern Ocean lacks hydrographic, shelf morphology and cryosphere conditions to create AABW varieties (Potter and Paren, 1985; Orsi et al., 1999)

It is important to highlight that the AABW formation processes by continental shelf waters convection in UR025.4 was a result of CDW-derived waters interacting with the ice edge in the Indian Ocean and Western Pacific sectors. This process is similar to that expected to occur in the real ocean, through the continental shelf convection and shelf-break interactions to create AABW (e.g. Williams et al., 2016).

3.3 Modelled and real ocean bottom water formation

Considering the three reanalysis investigated, two of them have formed AABW by open ocean deep convection. Starting from 1992, ECCO2 experiences an increase in the volume of WDW in the Weddell Sea, causing WDW isopycnal uplift until 2000, when WDW reaches the surface. After reaching the surface, WDW starts to interact with local sea ice and atmosphere, cooling and being slowly converted to WSDW during the first four years. By the winter of 2004, the heat transported by the

© Author(s) 2017. CC-BY 3.0 License.

WDW to the surface is enough to open a large polynya near the eastern limb of the Weddell Gyre, around 20°E. After the polynya opening, a more intense conversion of WDW to WSDW happens until 2008, when the latter starts to transform into WSBW. This four year delay is very close to the five years mean estimate of residence time for WDW in the Weddell Gyre before conversion to denser local AABW varieties (Fahrbach et al. 2011). After opening, the polynya expands every following winter, being present in the Weddell Sea, Indian Ocean and Western Pacific sectors of the Southern Ocean, and slightly weakening the sea ice concentration in the Ross Sea sector. That expansion leads to the formation of unrealistic 70% WSBW volume. A similar process occurs in SoSE, but in smaller space and temporal scales: WDW reaching the surface in the beginning of the reanalysis time series seem to hinder sea ice formation by the beginning of the winter and, as a result, an elongated polynya develops in the Weddell Sea during the winter of 2005. Even though in SoSE no estimate of WDW prior to 2005 exists, the high volume of this water mass near the surface in 2005 (Figure 8) points to the referred surface interaction as a trigger for the polynya opening. Therefore, it is clear that WDW volume increase near the surface causes a heat input in the upper layers during the 2004-2005 period in both of the previously mentioned reanalysis, eventually creating the large open ocean polynya in Weddell Sea.

Some other processes than the ones analyzed in this study may have influenced the polynya opening in abovementioned reanalysis. Parkinson (1983), while modelling the 1976 observed Weddell Polynya, noticed the wind patterns seemed to control whether the polynya would open or not in the simulation. Also, some simulations have shown that interaction of currents and eddies with the Maud Rise can alter the oceanic transport throughout the whole water Weddell Sea column, allowing heat exchange with sea ice and opening the Weddell Polynya (Holland, 2001a, 2001b). In a more recent study, Gordon et al. (2007) noticed that during long periods of negative Southern Annular Mode Index (Limpasuvan and Hartmann, 1999), the Weddell Sea has its sea ice formation and brine release enhanced, which destabilizes water column and allows a Weddell Polynya to happen. Lavergne et al., (2014) also states that the reduced occurrence of open ocean deep convection in Southern Ocean after 1950 is due to strong ice melt, enhancing Southern Ocean stratification, which shows that sea ice strong seasonality is an important trigger of polynya opening. In that matter, a recent study found that GISS-E2-R and GFDL-ESM22 ocean models from CIMP5 have their frequent deep connection events due to stronger seasonality of sea ice, enhancing winter brine release and homogenizing Weddell Sea water column, which allows deep convection to transfer heat to surface (Heuzé et al., 2013). According to Azaneu et al. (2014), ECCO2 also exhibits strong sea ice seasonality and that likely plays a role in the opening of the ECCO2 polynya. Despite none of those specific atmospheric and sea ice patterns were analyzed here, their manifestation allow WDW to rise to the surface leading deep convection and thus acting as triggers to polynya establishment. Moreover, several studies show the same pattern of WDW raising to surface, exchanging heat and opening the Weddell polynya in simulations (e.g. Hirabara et al. 2012; Martin et al. 2013; Cheon et al. 2015). It is also worth to mention that both ECCO2 and SoSE reanalysis use the same MITgcm ocean model, hence the polynya opening in Weddell Sea might be an expression of the same features of that circulation model. In addition, since SoSE polynya happens at the beginning of the reanalysis, we cannot rule out the possibility that SoSE is still adjusting from its initial settings.

© Author(s) 2017. CC-BY 3.0 License.

Although two of the reanalysis used in this study yielded open ocean polynya events forming AABW, the UR025.4 formed AABW in a completely different way. In this model, the first adjustment observed is a substantial rise of UCDW volume in the Indian Ocean sector. As seen in Fig. 10, this water entered the coastal regions of the Indian Ocean sector from surface up to the 250 m level, and interacted with the ice edge in that region, causing some of the ice to melt resulting initially in a freshening signal at the surface and intermediate layers in a relatively small area. That colder and fresher water resulting from the melting was transported westward through the ACoC. Because of the gradual heat lost along the way, sea ice formation happened eastern from the coastal UCDW signal, increasing the salinity over the denser LCDW positioned underneath and creating a high volume of DSW. DSW is then advected to the Weddell Sea by the ACoC system and offshore due to the buoyancy current formed Western Pacific sector. Although that process creates AABW through a mechanism similar to the real ocean, the AABW formation in Indian Ocean sector reported by Kitade et al. (2014) and Williams et al. (2016) still has significant differences. First, the real AABW formation in the Indian Ocean sector happens after the *modified-Circumpolar Deep Water* (mCDW) circulates deeper under the ice shelves surrounding Prydz and Vincennes bays, mixing with DSW created in coastal polynyas, acquiring a higher salt content and cooling down (Williams et al. 2016). The mCDW has neutral densities between 28.0 kg m^{-3} and 28.27 kg m^{-3}, hence a relatively small salt input and/or cooling can easily diminish mCDW buoyancy, thus forming AABW. In contrast, UR025.4 water mass in Prydz Bay (UCDW) is relatively warmer, less saline and lighter than mCDW, causing a balance between immediate melting under sea ice and freezing as the water circulates along the coast. This balance releases brine over LCDW, creating very saline LCDW and AABW varieties. In addition, the AABW formation in UR025.4 occurs mainly by salinization and as result, the final AABW has substantially higher salinity than expected. Also, the density increase by this salinization and the relative low density of UCDW causes a baroclinic current that speeds up the ACoC, and creates a creates a current component directed offshore that export DSW downslope from the shelf.

The results of AABW volume in UR025.4 suggest that the eastern Southern Ocean plays an important role on the AABW formation in this simulation. In real ocean, Meredith et al. (2000) pointed out that the properties of the AABW varieties in the Weddell Sea are likely modified by dense bottom water advection from the Indian Ocean sector, such as happened in UR025.4. Also, Jullion et al. (2014) found that the great export of bottom water varieties from Weddell Gyre is largely due to recycling of AABW produced in Indian Ocean sector. Finally, Couldrey et al. (2013) indicated that the export and properties change of AABW varieties in the Weddell Sea are caused due to the entrainment of CDW around the Prydz Bay, being further advected into the Weddell Gyre. Therefore, the process of AABW formation in UR025.4 accurately mimics the bottom water formation reported by the previously mentioned articles.

The distinct AABW formation process present in UR025.4 might be caused by the advection of CDW-derived waters happened in an eastern region of Antarctica, and not in the Weddell Sea. Eastern Antarctic deep waters are less dense then deep waters in Weddell Sea, and hence waters flowing along isopycnals flow up when reaching Weddell Sea. This natural upward shift of pycnoclines towards the center of Weddell Gyre creates a region with low sea ice concentration and thickness around the center of the gyre (de Steur et al., 2007). Thus, warm water volume increments in deep Weddell layers

© Author(s) 2017. CC-BY 3.0 License.

are potentially more destructive to sea ice than in deep waters of Indian Ocean sector. In fact, Timmermann and Beckmann (2004), while trying to reproduce accurately that so-called *warm water halo*, found an enhanced vertical heat exchange with sea ice leading to opening an open ocean polynya in the Weddell Sea.

4 Summary and Conclusions

Deep convection in open ocean polynyas, together with sea ice and ice-shelf representation, has been pointed as a frequent causes of spurious AABW formation and/or a source of erroneous ocean representation in non-assimilatory OGCM's (e.g. Kerr et al., 2009b; Meccia et al., 2013; Stössel et al., 2002). Spurious open ocean deep convection create AABW through a rather abrupt mechanism, enhancing bottom layer ventilation and heat/carbon uptake, which inserts errors in climate estimates (e.g. Heuzé et al., 2013). Propagation of spurious open ocean deep convection in Southern Ocean simulations can go even further, causing warming of abyssal layer, cooling of surface waters and atmospheric warming (Latif et al. 2013; Pedro et al. 2016). The mechanisms of bottom water formation in some of the reanalysis investigated here agree with those ideas: two of the three reanalysis created AABW by deep convection associated to areas of large open ocean polynyas. In both ECCO2 and SoSE the presence of WDW at surface hinders sea ice formation during winter, and triggers a deep convection event, which creates AABW by cooling. In those two reanalysis, the mechanism of AABW formation resulted in erroneous representations of the Southern Ocean, such as high AABW volumes and lower sea ice concentrations and thicknesses, reinforcing that open ocean deep convection inserts errors in the simulation. Even though the appearance of open ocean polynyas in models without assimilation are a well-known modelling issue, the opening of the Weddell Polynya in reanalysis products is a less expected feature. Since reanalysis products are meant to be precise representations of ocean state due to the assimilation of observations, the appearance of spurious AABW formation by open ocean deep convection shows that the assimilation of sea ice concentrations has not been enough to hinder the appearance of open ocean polynyas.

One of the ocean reanalysis in this study (i.e. UR025.4) created AABW in a different way. Biggest AABW formation in UR025.4 happened mainly eastern from Weddell Sea sector, agreeing with real Southern Ocean evidences (e.g. Meredith et al., 2000; Jullion et al., 2014). The entrainment of UCDW in this reanalysis Indian Ocean sector, created an equilibrium between melting and freezing that favoured LCDW salinization, leading to coastal deep convection. The salinization created DSW that mixed with LCDW formed AABW while flowing downslope. This mechanism of bottom water formation is dynamically similar to the real ocean formation of AABW since it depicts both the spilling of DSW off the continental shelf, and the exportation to open ocean, processes that do occur in Indian sector of real Southern Ocean (Kitade et al. 2014; Williams et al. 2016). Although this mechanism is closer to the real bottom water formation in eastern Southern Ocean, some anomalous dynamic processes were created by the sea ice balance. First, the density gradient seem to enhance ACoC circulation by creating a buoyancy current. The enhanced advection by the buoyancy current accumulates sea ice around the Antarctic Peninsula, creating unrealistically high sea ice thicknesses, which in turn induces the spurious deep and bottom layers salinization reported by Dotto et al. (2014). Low salinity and temperature waters advected from Indian Ocean sector to

© Author(s) 2017. CC-BY 3.0 License.

Weddell Sea also contribute to AABW formation in the later sector due to its higher freezing point. Nevertheless, the somewhat accurate dynamical representation of the AABW formation in UR025.4 is an advance in Southern Ocean representation in OGCM's and ocean reanalysis products (e.g. Kerr et al. 2009b, 2012b; Azaneu et al. 2014, Dotto et al., 2014), since it shows that ocean reanalysis advanced frameworks are getting closer to efficiently represent AABW formation. Furthermore, the substantial differences between the UR025.4 process and real ocean AABW formation in Indian Ocean sector, shows that improvements in simulations of AABW formation are still necessary to better represent the lower limb of the AMOC.

5 Acknowledgements

This study is a contribution to the activities of the Brazilian High Latitudes Oceanography Group (GOAL) and the Brazilian National Institute of Science and Technology of Cryosphere (INCT-CRIOSFERA, 465680/2014-3). GOAL has been funded by the Brazilian Antarctic Program (PROANTAR) through the Brazilian Ministry of the Environment (MMA), the Brazilian Ministry of Science, Technology and Innovation (MCTI), and the Council for Research and Scientific Development of Brazil (CNPq; 550370/2002-1; 520189/2006-0; 556848/2009-8; 405869/2013-4). W.A. acknowledges the financial support from the CAPES Foundation. M.M.M and R.K acknowledge CNPq fellowships 306896/2015-0 and 302604/2015-4, respectively .We thank specially the NSIDC and research groups responsible for developing the ECCO2, SoSE and UR025.4, for making their datasets available online.

References

Abernathey, R. P., Cerovecki, I., Holland, P. R., Newsom, E., Mazloff, M. and Talley, L. D.: Water-mass transformation by sea ice in the upper branch of the Southern Ocean overturning, Nat. Geosci, advance on [online] Available from: http://dx.doi.org/10.1038/ngeo2749, 2016.

Azaneu, M., Kerr, R., Mata, M. M. and Garcia, C. A. E.: Trends in the deep Southern Ocean (1958-2010): Implications for Antarctic Bottom Water properties and volume export, J. Geophys. Res. Ocean., 118(9), 4213–4227, doi:10.1002/jgrc.20303, 2013.

Azaneu, M., Kerr, R. and Mata, M. M.: Assessment of the representation of Antarctic Bottom Water properties in the ECCO2 reanalysis, Ocean Sci., 10(6), 923–946, doi:10.5194/os-10-923-2014, 2014.

Berge-Nguyen, M., Cazenave, A., Lombard, A., Llovel, W., Viarre, J. and Cretaux, J. F.: Reconstruction of past decades sea level using thermosteric sea level, tide gauge, satellite altimetry and ocean reanalysis data, Glob. Planet. Change, 62(1–2), 1–13, doi:http://dx.doi.org/10.1016/j.gloplacha.2007.11.007, 2008.

© Author(s) 2017. CC-BY 3.0 License.

Carmack, E. C. and Foster, T. D.: On the flow of water out of the Weddell Sea, Deep Sea Res. Oceanogr. Abstr., 22(11), 711–724, doi:http://dx.doi.org/10.1016/0011-7471(75)90077-7, 1975.

Carsey, F. D.: Microwave Observation of the Weddell Polynya, Mon. Weather Rev., 108(12), 2032–2044, doi:10.1175/1520-0493(1980)108<2032:MOOTWP>2.0.CO;2, 1980.

Carton, J. A., Giese, B. S. and Grodsky, S. A.: Sea level rise and the warming of the oceans in the Simple Ocean Data Assimilation (SODA) ocean reanalysis, J. Geophys. Res. Ocean., 110(C9), n/a--n/a, doi:10.1029/2004JC002817, 2005.

Cheon, W. G., Lee, S.-K., Gordon, A. L., Liu, Y., Cho, C.-B. and Park, J. J.: Replicating the 1970s' Weddell Polynya using a coupled ocean-sea ice model with reanalysis surface flux fields, Geophys. Res. Lett., 42(13), 5411–5418, doi:10.1002/2015GL064364, 2015.

Close, S. E. and Goosse, H.: Entrainment-driven modulation of Southern Ocean mixed layer properties and sea ice variability in CMIP5 models, J. Geophys. Res. Ocean., 118(6), 2811–2827, doi:10.1002/jgrc.20226, 2013.

Comiso, J. C. and Gordon, A. L.: Recurring polynyas over the Cosmonaut Sea and the Maud Rise, J. Geophys. Res. Ocean., 92(C3), 2819–2833, doi:10.1029/JC092iC03p02819, 1987.

Couldrey, M. P., Jullion, L., Naveira Garabato, A. C., Rye, C., Herráiz-Borreguero, L., Brown, P. J., Meredith, M. P. and Speer, K. L.: Remotely induced warming of Antarctic Bottom Water in the eastern Weddell gyre, Geophys. Res. Lett., 40(11), 2755–2760, doi:10.1002/grl.50526, 2013.

Dee, D. P., Uppala, S. M., Simmons, A. J., Berrisford, P., Poli, P., Kobayashi, S., Andrae, U., Balmaseda, M. A., Balsamo, G., Bauer, P., Bechtold, P., Beljaars, A. C. M., van de Berg, L., Bidlot, J., Bormann, N., Delsol, C., Dragani, R., Fuentes, M., Geer, A. J., Haimberger, L., Healy, S. B., Hersbach, H., Hólm, E. V, Isaksen, L., Kållberg, P., Köhler, M., Matricardi, M., McNally, A. P., Monge-Sanz, B. M., Morcrette, J.-J., Park, B.-K., Peubey, C., de Rosnay, P., Tavolato, C., Thépaut, J.-N. and Vitart, F.: The ERA-Interim reanalysis: configuration and performance of the data assimilation system, Q. J. R. Meteorol. Soc., 137(656), 553–597, doi:10.1002/qj.828, 2011.

Dotto, T. S., Kerr, R., Mata, M. M., Azaneu, M., Wainer, I., Fahrbach, E. and Rohardt, G.: Assessment of the structure and variability of weddell sea water masses in distinct ocean reanalysis products, Ocean Sci., 10(3), 523–546, doi:10.5194/os-10-523-2014, 2014.

Fahrbach, E., Hoppema, M., Rohardt, G., Schröder, M. and Wisotzki, A.: Decadal-scale variations of water mass properties in the deep Weddell Sea, Ocean Dyn., 54, 77–91, doi:10.1007/s10236-003-0082-3, 2004.

Fahrbach, E., Hoppema, M., Rohardt, G., Boebel, O., Klatt, O. and Wisotzki, A.: Warming of deep and abyssal water masses along the Greenwich meridian on decadal time scales : The Weddell gyre as a heat buffer, Deep. Res. Part II, 58(25–26), 2509–2523, doi:10.1016/j.dsr2.2011.06.007, 2011.

Ferry, N., Barnier, B., Garric, G., Haines, K., Masina, S., Parent, L., Storto, A., Valdivieso, M. and Guinehut, S.: Nemo: The

© Author(s) 2017. CC-BY 3.0 License.

modelling engine of global ocean reanalysis, Mercat. Ocean Q. Newsl., 46, 46–59, 2012.

Fichefet, T. and Maqueda, M. A. M.: Sensitivity of a global sea ice model to the treatment of ice thermodynamics and dynamics, J. Geophys. Res., 102, 1997.

Foldvik, A., Gammelsrød, T. and Tørresen, T.: Circulation and Water Masses on the Southern Weddell Sea Shelf, in Oceanology of the Antarctic Continental Shelf, pp. 5–20, American Geophysical Union., 1985.

Foster, T. D. and Carmack, E. C.: Frontal zone mixing and Antarctic Bottom water formation in the southern Weddell Sea, Deep Sea Res. Oceanogr. Abstr., 23(4), 301–317, doi:10.1016/0011-7471(76)90872-X, 1976.

Franco, B. C., Mata, M. M., Piola, A. R. and Garcia, C. A. E.: Northwestern Weddell Sea deep outflow into the Scotia Sea during the austral summers of 2000 and 2001 estimated by inverse methods, Deep Sea Res. Part I Oceanogr. Res. Pap., 54(10), 1815–1840, doi:http://dx.doi.org/10.1016/j.dsr.2007.06.003, 2007.

Gordon, A. L.: Deep Antarctic Convection West of Maud Rise, J. Phys. Oceanogr., 8(4), 600–612, doi:10.1175/1520-0485(1978)008<0600:DACWOM>2.0.CO;2, 1978.

Gordon, A. L.: Weddell deep water variability, J. Mar. Res, 40, 199–217, 1982.

Gordon, A. L., Visbeck, M. and Comiso, J. C.: A possible link between the Weddell Polynya and the southern annular mode, J. Clim., 20(11), 2558–2571, doi:10.1175/JCLI4046.1, 2007.

Heuzé, C., Heywood, K. J., Stevens, D. P. and Ridley, J. K.: Southern Ocean bottom water characteristics in CMIP5 models, Geophys. Res. Lett., 40(7), 1409–1414, doi:10.1002/grl.50287, 2013.

Hibler, W. D.: Modeling a Variable Thickness Sea Ice Cover, Mon. Weather Rev., 108, 1943–1973, doi:10.1175/1520-0493(1980)108<1943:MAVTSI>2.0.CO;2., 1980.

Hirabara, M., Tsujino, H., Nakano, H. and Yamanaka, G.: Formation mechanism of the Weddell Sea Polynya and the impact on the global abyssal ocean, J. Oceanogr., 68(5), 771–796, doi:10.1007/s10872-012-0139-3, 2012.

Holland, D. M.: Explaining the Weddell Polynya-a Large Ocean Eddy Shed at Maud Rise, Science (80). 292(5522), 1697–1700, doi:10.1126/science.1059322, 2001a.

Holland, D. M.: Transient sea-ice polynya forced by oceanic flow variability , Prog. Oceanogr. , 48(4), 403–460, doi:10.1016/S0079-6611(01)00010-6 , 2001b.

Jackett, D. R. and McDougall, T. J.: A Neutral Density Variable for the World's Oceans, J. Phys. Oce, 27(1968), 237–263, 1997.

Jullion, L., Garabato, A. C. N., Bacon, S., Meredith, M. P., Brown, P. J., Torres-Valdés, S., Speer, K. G., Holland, P. R., Dong, J., Bakker, D., Hoppema, M., Loose, B., Venables, H. J., Jenkins, W. J., Messias, M.-J. and Fahrbach, E.: The contribution of the Weddell Gyre to the lower limb of the Global Overturning Circulation, J. Geophys. Res. Ocean., 119(6),

© Author(s) 2017. CC-BY 3.0 License.

3357–3377, doi:10.1002/2013JC009725, 2014.

Kerr, R., Mata, M. M. and Garcia, C. A. E.: On the temporal variability of the Weddell Sea Deep Water masses, Antarct. Sci., 21(4), 383–400, doi:10.1017/S0954102009001990, 2009a.

Kerr, R., Wainer, I. and Mata, M. M.: Representation of the Weddell Sea deep water masses in the ocean component of the NCAR-CCSM model, Antarct. Sci., 21(3), 301–312, doi:10.1017/S0954102009001825, 2009b.

Kerr, R., Heywood, K. J., Mata, M. M. and Garcia, C. A. E.: On the outflow of dense water from the Weddell and Ross Seas in OCCAM model, Ocean Sci., 8(3), 369–388, doi:10.5194/os-8-369-2012, 2012a.

Kerr, R., Wainer, I., Mata, M. M. and Garcia, C. a. E.: Quantifying Antarctic deep waters in SODA reanalysis product, Pesqui. Antártica Bras., 59, 47–59, 2012b.

Killworth, P. D.: Deep convection in the World Ocean, Rev. Geophys., 21(1), 1, doi:10.1029/RG021i001p00001, 1983.

Kitade, Y., Shimada, K., Tamura, T., Williams, G. D., Aoki, S., Fukamachi, Y., Roquet, F., Hindell, M., Ushio, S. and Ohshima, K. I.: Antarctic Bottom Water production from the Vincennes Bay Polynya, East Antarctica, Geophys. Res. Lett., 41(10), 3528–3534, doi:10.1002/2014GL059971, 2014.

Köhl, A. and Stammer, D.: Decadal Sea Level Changes in the 50-Year GECCO Ocean Synthesis, J. Clim., 21(9), 1876–1890, doi:10.1175/2007JCLI2081.1, 2008.

Latif, M., Martin, T. and Park, W.: Southern ocean sector centennial climate variability and recent decadal trends, J. Clim., 26(19), 7767–7782, doi:10.1175/JCLI-D-12-00281.1, 2013.

Lavergne, C. De, Palter, J. B., Galbraith, E. D., Bernardello, R. and Marinov, I.: Cessation of deep convection in the open Southern Ocean under anthropogenic climate change, Nat. Clim. Chang., 4(4), 0–4, doi:10.1038/NCLIMATE2132, 2014.

Lee, T., Awaji, T., Balmaseda, M. A., Greiner, E. and Stammer, D.: Ocean State Estimation for Climate Research, Oceanography, 22 [online] Available from: http://dx.doi.org/10.5670/oceanog.2009.74, 2009.

Limpasuvan, V. and Hartmann, D. L.: Eddies and the annular modes of climate variability, Geophys. Res. Lett., 26(20), 3133–3136, doi:10.1029/1999GL010478, 1999.

Marshall, J., Adcroft, A., Hill, C., Perelman, L. and Heisey, C.: A finite-volume , incompressible Navier Stokes model for studies of the ocean on parallel computers, , 102, 5753–5766, 1997.

Marsland, S. J., Haak, H., Jungclaus, J. H., Latif, M. and Röske, F.: The Max-Planck-Institute global ocean/sea ice model with orthogonal curvilinear coordinates, Ocean Model., 5(2), 91–127, doi:http://dx.doi.org/10.1016/S1463-5003(02)00015-X, 2003.

Martin, T., Park, W. and Latif, M.: Multi-centennial variability controlled by Southern Ocean convection in the Kiel Climate Model, Clim. Dyn., 40(7), 2005–2022, doi:10.1007/s00382-012-1586-7, 2013.

© Author(s) 2017. CC-BY 3.0 License.

Massonnet, F., Fichefet, T., Goosse, H., Vancoppenolle, M., Mathiot, P. and König Beatty, C.: On the influence of model physics on simulations of Arctic and Antarctic sea ice, Cryosph., 5(3), 687–699, doi:10.5194/tc-5-687-2011, 2011.

Mazloff, M. R., Heimbach, P. and Wunsh, C.: An Eddy-Permitting Southern Ocean State Estimate, J. Phys. Oceanogr., 40, 880–899, doi:10.1175/2009JPO4236.1, 2010.

Meccia, V., Wainer, I., Tonelli, M. and Curchitser, E.: Coupling a thermodynamically active ice shelf to a regional simulation of the Weddell Sea, Geosci. Model Dev., 6(4), 1209–1219, doi:10.5194/gmd-6-1209-2013, 2013.

Menemenlis, D., Campin, J. M., Heimbach, P., Hill, C., Lee, T., Nguyen, A., Schodlok, M. and Zhang, H.: ECCO2: High resolution global ocean and sea ice data synthesis, Mercat. Ocean Q. Newsl., 31, 13–21, 2008.

Meredith, M. P., Locarnini, R. A., Van Scoy, K. A., Watson, A. J., Heywood, K. J. and King, B. A.: On the sources of Weddell Gyre Antarctic Bottom Water, J. Geophys. Res. Ocean., 105(C1), 1093–1104, doi:10.1029/1999JC900263, 2000.

Morales Maqueda, M. A., Willmott, A. J. and Biggs, N. R. T.: Polynya Dynamics: a Review of Observations and Modeling, Rev. Geophys., 42(1), n/a--n/a, doi:10.1029/2002RG000116, 2004.

Naveira Garabato, A. C., Heywood, K. J. and Stevens, D. P.: Modification and pathways of Southern Ocean Deep Waters in the Scotia Sea, Deep Sea Res. Part I Oceanogr. Res. Pap., 49(4), 681–705, doi:http://dx.doi.org/10.1016/S0967-0637(01)00071-1, 2002.

Nicholls, K. W., Østerhus, S., Makinson, K., Gammelsrød, T. and Fahrbach, E.: Ice-ocean processes over the continental shelf of the southern Weddell Sea, Antarctica: A review, Rev. Geophys., 47(3), doi:10.1029/2007RG000250, 2009.

Orsi, A. H., Johnson, G. C. and Bullister, J. L.: Circulation, mixing, and production of Antarctic Bottom Water, Prog. Oceanogr., 43(1), 55–109, doi:http://dx.doi.org/10.1016/S0079-6611(99)00004-X, 1999.

Parkinson, C. L.: On the Development and Cause of the Weddell Polynya in a Sea Ice Simulation, J. Phys. Oceanogr., 13(3), 501–511, doi:10.1175/1520-0485(1983)013<0501:OTDACO>2.0.CO;2, 1983.

Parkinson, C. L. and Cavalieri, D. J.: Antarctic sea ice variability and trends , 1979 – 2010, , 871–880, doi:10.5194/tc-6-871-2012, 2012.

Pedro, J. B., Martin, T., Steig, E. J., Jochum, M., Park, W. and Rasmussen, S. O.: Southern Ocean deep convection as a driver of Antarctic warming events, Geophys. Res. Lett., 43(5), 2192–2199, doi:10.1002/2016GL067861, 2016.

Potter, J. R. and Paren, J. G.: Interaction Between Ice Shelf and Ocean in George VI Sound, Antarctica, in Oceanology of the Antarctic Continental Shelf, pp. 35–58, American Geophysical Union., 1985.

Purkey, S. G. and Johnson, G. C.: Global contraction of Antarctic Bottom Water between the 1980s and 2000s, J. Clim., 25(17), 5830–5844, doi:10.1175/JCLI-D-11-00612.1, 2012.

Schiller, A., Oke, P. R., Brassington, G., Entel, M., Fiedler, R., Griffin, D. A. and Mansbridge, J. V.: Eddy-resolving ocean

© Author(s) 2017. CC-BY 3.0 License.

circulation in the Asian–Australian region inferred from an ocean reanalysis effort, Prog. Oceanogr., 76(3), 334–365, doi:http://dx.doi.org/10.1016/j.pocean.2008.01.003, 2008.

Serazin, G.: An approximate Neutral Density variable for the world's oceans, École Centrale de Lyon., 2011.

Shaffrey, L. C., Stevens, I., Norton, W. A., Roberts, M. J., Vidale, P. L., Harle, J. D., Jrrar, A., Stevens, D. P., Woodage, M. J., Demory, M. E., Donners, J., Clark, D. B., Clayton, A., Cole, J. W., Wilson, S. S., Connolley, W. M., Davies, T. M., Iwi, A. M., Johns, T. C., King, J. C., New, A. L., Slingo, J. M., Slingo, A., Steenman-Clark, L. and Martin, G. M.: U.K. HiGEM: The New U.K. High-Resolution Global Environment Model—Model Description and Basic Evaluation, J. Clim., 22(8), 1861–1896, doi:10.1175/2008JCLI2508.1, 2009.

de Steur, L., Holland, D. M., Muench, R. D. and McPhee, M. G.: The warm-water "Halo" around Maud Rise: Properties, dynamics and Impact, Deep Sea Res. Part I Oceanogr. Res. Pap., 54(6), 871–896, doi:http://dx.doi.org/10.1016/j.dsr.2007.03.009, 2007.

Storkey, D., Blockley, E. W., Furner, R., Guiavarc'h, C., Lea, D., Martin, M. J., Barciela, R. M., Hines, A., Hyder, P. and R., S. J.: Forecasting the ocean state using NEMO:The new FOAM system, J. Oper. Oceanogr., 8778(September), doi:10.1080/1755876X.2010.11020109, 2010.

Stössel, A., Yang, K. and Kim, S.-J.: On the Role of Sea Ice and Convection in a Global Ocean Model, J. Phys. Oceanogr., 32(4), 1194–1208, doi:10.1175/1520-0485(2002)032<1194:OTROSI>2.0.CO;2, 2002.

Talley, L. D.: Closure of the Global Overturning Circulation Through the Indian, Pacific, and Southern Oceans: Schematics and Transports, Oceanography, 26 [online] Available from: http://dx.doi.org/10.5670/oceanog.2013.07, 2013.

Timmermann, R. and Beckmann, A.: Parameterization of vertical mixing in the Weddell Sea, Ocean Model., 6(1), 83–100, doi:http://dx.doi.org/10.1016/S1463-5003(02)00061-6, 2004.

Whitworth, T. and Orsi, A. H.: Antarctic Bottom Water production and export by tides in the Ross Sea, Geophys. Res. Lett., 33(12), n/a--n/a, doi:10.1029/2006GL026357, 2006.

Williams, G. D., Bindoff, N. L., Marsland, S. J. and Rintoul, S. R.: Formation and export of dense shelf water from the Adélie Depression, East Antarctica, J. Geophys. Res. Ocean., 113(C4), doi:10.1029/2007JC004346, 2008.

Williams, G. D., Herraiz-Borreguero, L., Roquet, F., Tamura, T., Ohshima, K. I., Fukamachi, Y., Fraser, A. D., Gao, L., Chen, H., McMahon, C. R., Harcourt, R. and Hindell, M.: The suppression of Antarctic bottom water formation by melting ice shelves in Prydz Bay, Nat. Commun., 7, 12577 [online] Available from: http://dx.doi.org/10.1038/ncomms12577, 2016.

Wunsch, C., Ponte, R. M. and Heimbach, P.: Decadal Trends in Sea Level Patterns: 1993–2004, J. Clim., 20(24), 5889–5911, doi:10.1175/2007JCLI1840.1, 2007.

Zhang, J., Hibler, W. D., Steele, M. and Rothrock, D. A.: Arctic Ice – Ocean Modeling with and without Climate Restoring,

© Author(s) 2017. CC-BY 3.0 License.

J. Phys. Oceanogr., 28, 191–217, 1998.

Zhu, J., Huang, B. and Balmaseda, M. A.: An ensemble estimation of the variability of upper-ocean heat content over the tropical Atlantic Ocean with multi-ocean reanalysis products, Clim. Dyn., 39(3), 1001–1020, doi:10.1007/s00382-011-1189-8, 2012.

Ocean Sci. Discuss., doi:10.5194/os-2017-9, 2017
Manuscript under review for journal Ocean Sci.
Discussion started: 17 March 2017
© Author(s) 2017. CC-BY 3.0 License.

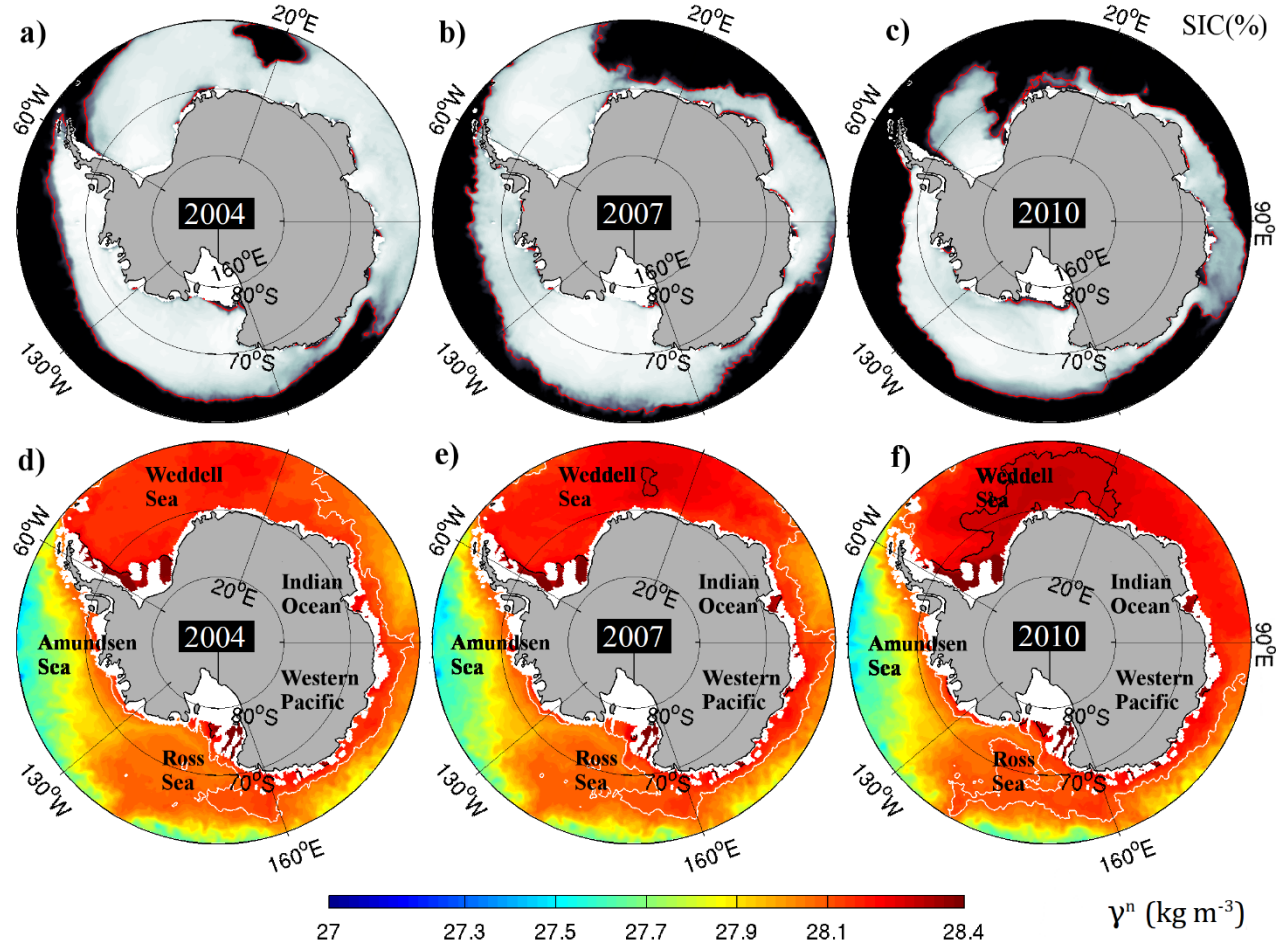

Figure 1: Top: Mean ECCO2 sea ice concentration (SIC; %) in November of (a) 2004, (b) 2007 and (c) 2010. Red contours delineate the line of 30% of SIC, which is considered here as the border of the polynya. Black straight lines separate each Southern Ocean sectors analyzed (see text for details). Bottom: Mean neutral density filled contours at 700 m in November of (d) 2004, (e) 2007 and (f) 2010. The white lines delineate the 28.1 kg m^{-3} neutral density isopycnal (WDW upper boundary), whereas the black lines mark the 28.27 kg m^{-3} isopycnal (WSDW upper boundary).

Ocean Sci. Discuss., doi:10.5194/os-2017-9, 2017
Manuscript under review for journal Ocean Sci.
Discussion started: 17 March 2017
© Author(s) 2017. CC-BY 3.0 License.

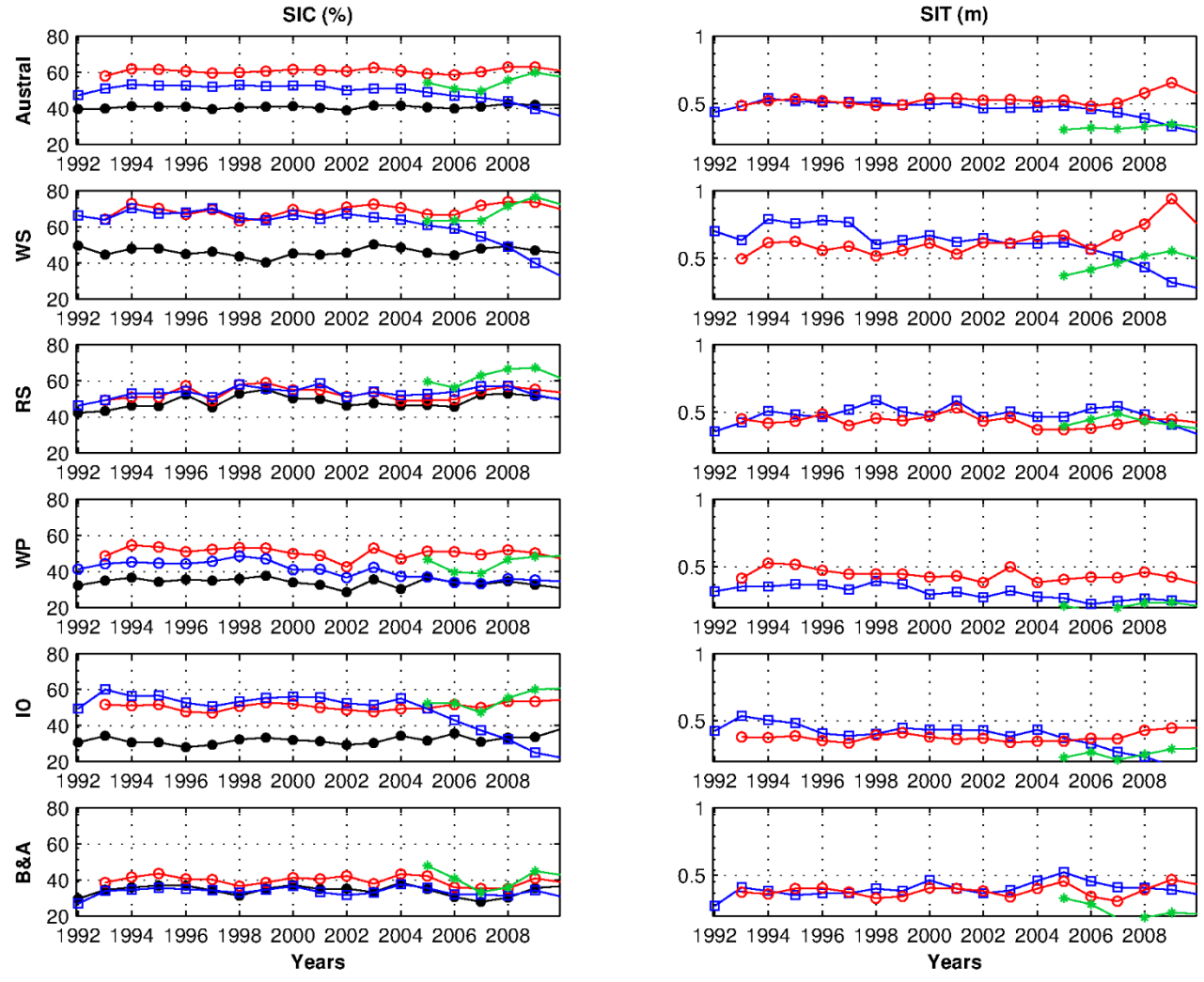

Figure 2: Annual mean (left) sea ice concentration (SIC; %) and (right) sea ice thickness (SIT; m) of each sector of the Southern Ocean. Red (○), green (*), and blue (□) symbol-lines represent the annual mean time series for UR025.4, SoSE, and ECCO2, respectively. Black line (●) represents the mean sea ice concentration from NSIDC satellite observations. Southern Ocean sectors are labeled as Weddell Sea (WS), Ross Sea (RS), Western Pacific (WP), Indian Ocean (IO) and Bellingshausen and Amundsen seas (B&A).

Ocean Sci. Discuss., doi:10.5194/os-2017-9, 2017
Manuscript under review for journal Ocean Sci.
Discussion started: 17 March 2017
© Author(s) 2017. CC-BY 3.0 License.

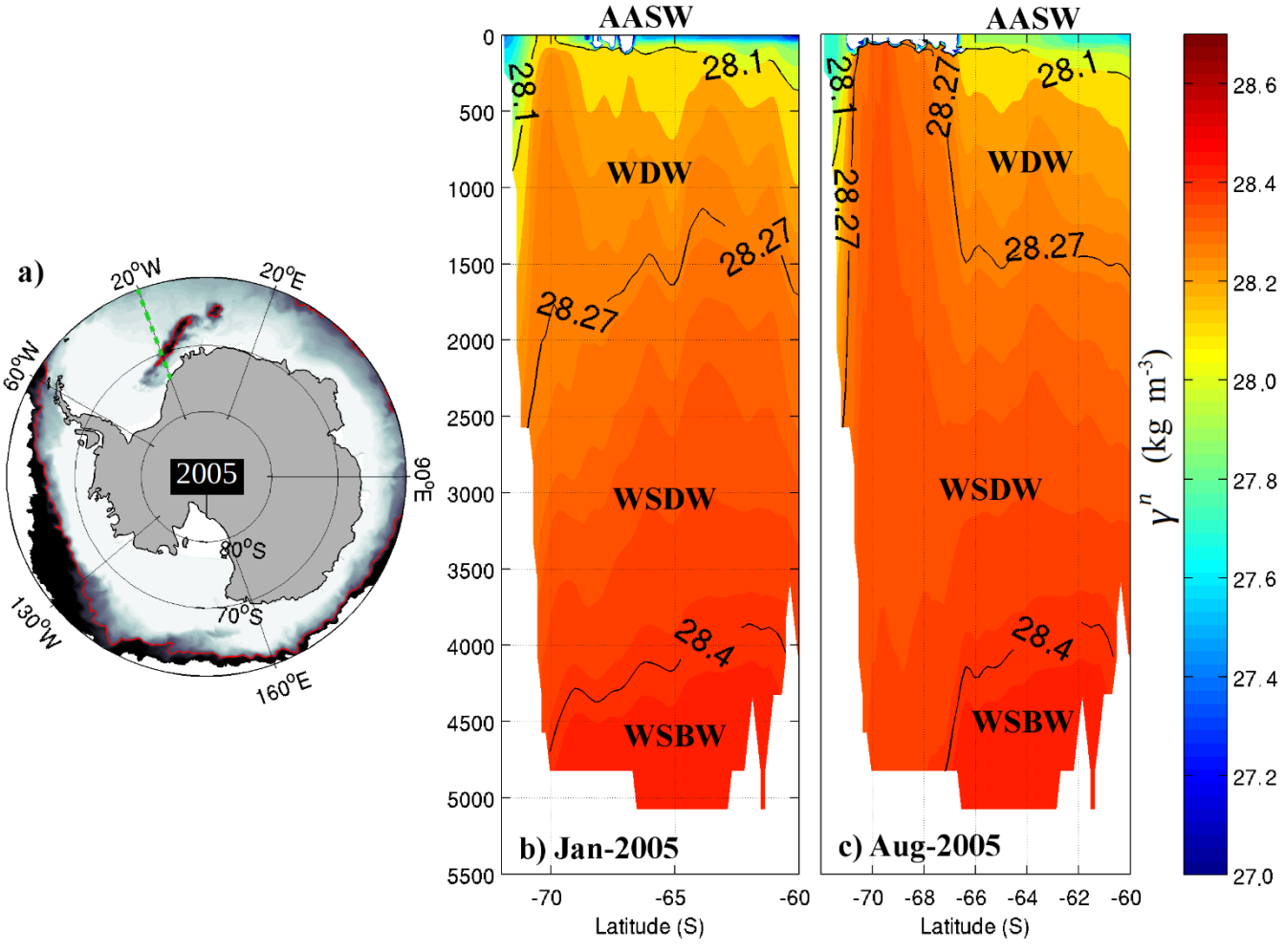

Figure 3: (a) Map with sea ice concentration of SoSE in August 2005 showing the polynya. The reanalysis section used in (b) and (c) is marked by the green dashed line. Black contours in (a) are areas with 0% sea ice concentration. The red line in (a) marks the 30% of sea ice concentration margin, as the border of the polynya. Neutral Density vertical distribution at 20°W during (b) January 2005 and (c) August 2005, respectively. Neutral density contours of 28.1 kg m^{-3}, 28.27 kg m^{-3} and 28.4 kg m^{-3} distinct the layers of AASW/WDW, WDW/WSDW, and WSDW/WSBW, respectively. See text for acronyms.

Ocean Sci. Discuss., doi:10.5194/os-2017-9, 2017
Manuscript under review for journal Ocean Sci.
Discussion started: 17 March 2017
© Author(s) 2017. CC-BY 3.0 License.

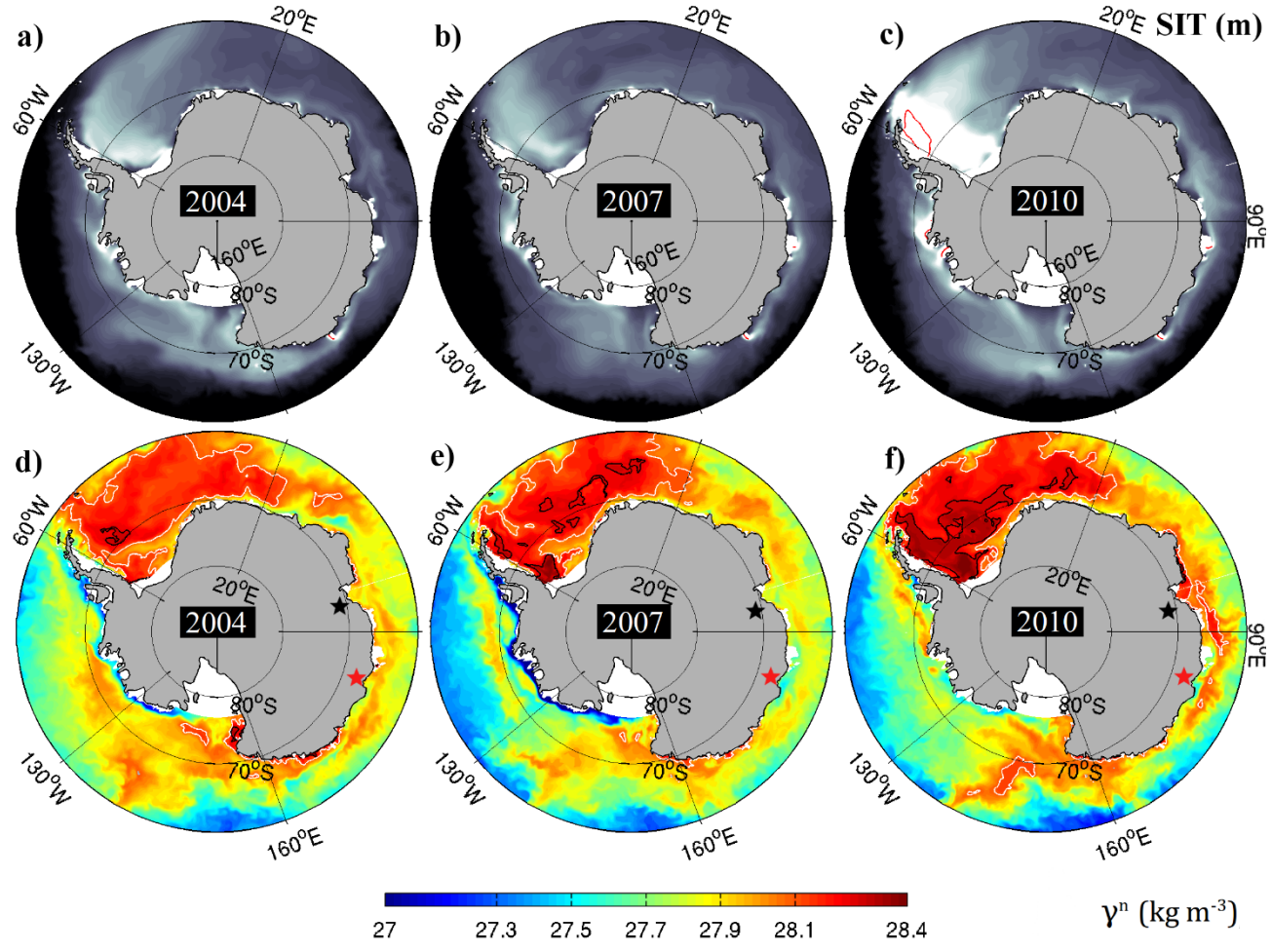

Figure 4: Top: Monthly sea ice thickness (SIT; m) of UR025.4 in September of (a) 2004, (b) 2007, and (c) 2010 . The red line marks the 3.5 m sea ice thickness, whereas the black contours are areas without sea ice. Bottom: Neutral density contours at 700 m depth in September of (d) 2004, (e) 2007, and (f) 2010. The white lines delineate the 28.1 kg m^{-3} neutral density isopycnal (WDW upper boundary), whereas the black lines mark the 28.27 kg m^{-3} isopycnal (WSDW upper boundary).

Ocean Sci. Discuss., doi:10.5194/os-2017-9, 2017
Manuscript under review for journal Ocean Sci.
Discussion started: 17 March 2017
© Author(s) 2017. CC-BY 3.0 License.

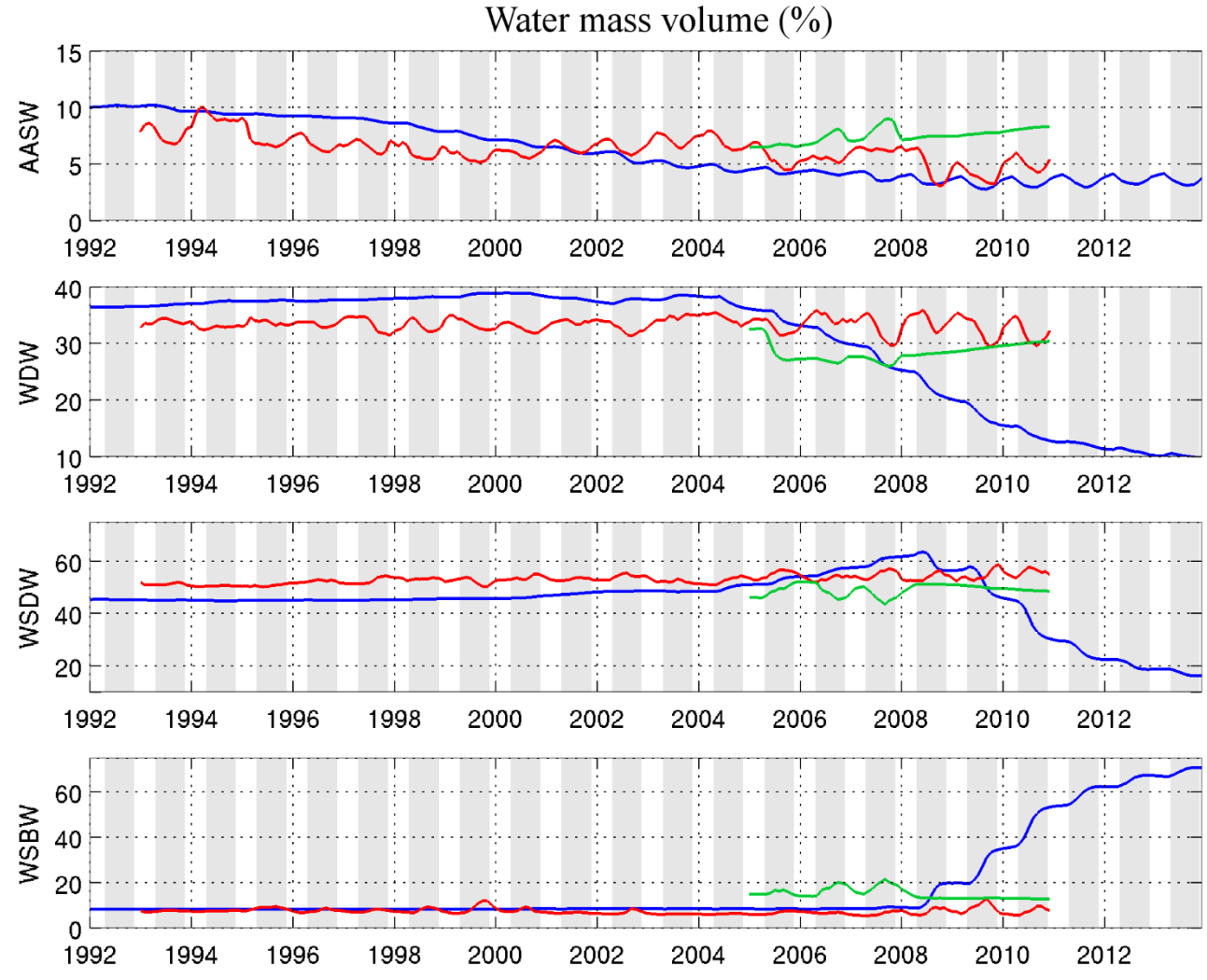

Figure 5: Volume percentage of Weddell Sea sector occupied by the following water mass: *Antarctic Surface Water* (AASW; γ^n<28.1 kg m^{-3}), *Warm Deep Water* (WDW; 28.27 kg m^{-3}< γ^n < 28.10 kg m^{-3}), *Weddell Sea Deep Water* (WSDW; 28.40 kg m^{-3}< γ^n < 28.27 kg m^{-3}) and *Weddell Sea Bottom Water* (WSBW; γ^n > 28.40 kg m^{-3}). The red, blue, and green lines depict UR025.4, ECCO2, and SoSE reanalysis, respectively.

Ocean Sci. Discuss., doi:10.5194/os-2017-9, 2017
Manuscript under review for journal Ocean Sci.
Discussion started: 17 March 2017
© Author(s) 2017. CC-BY 3.0 License.

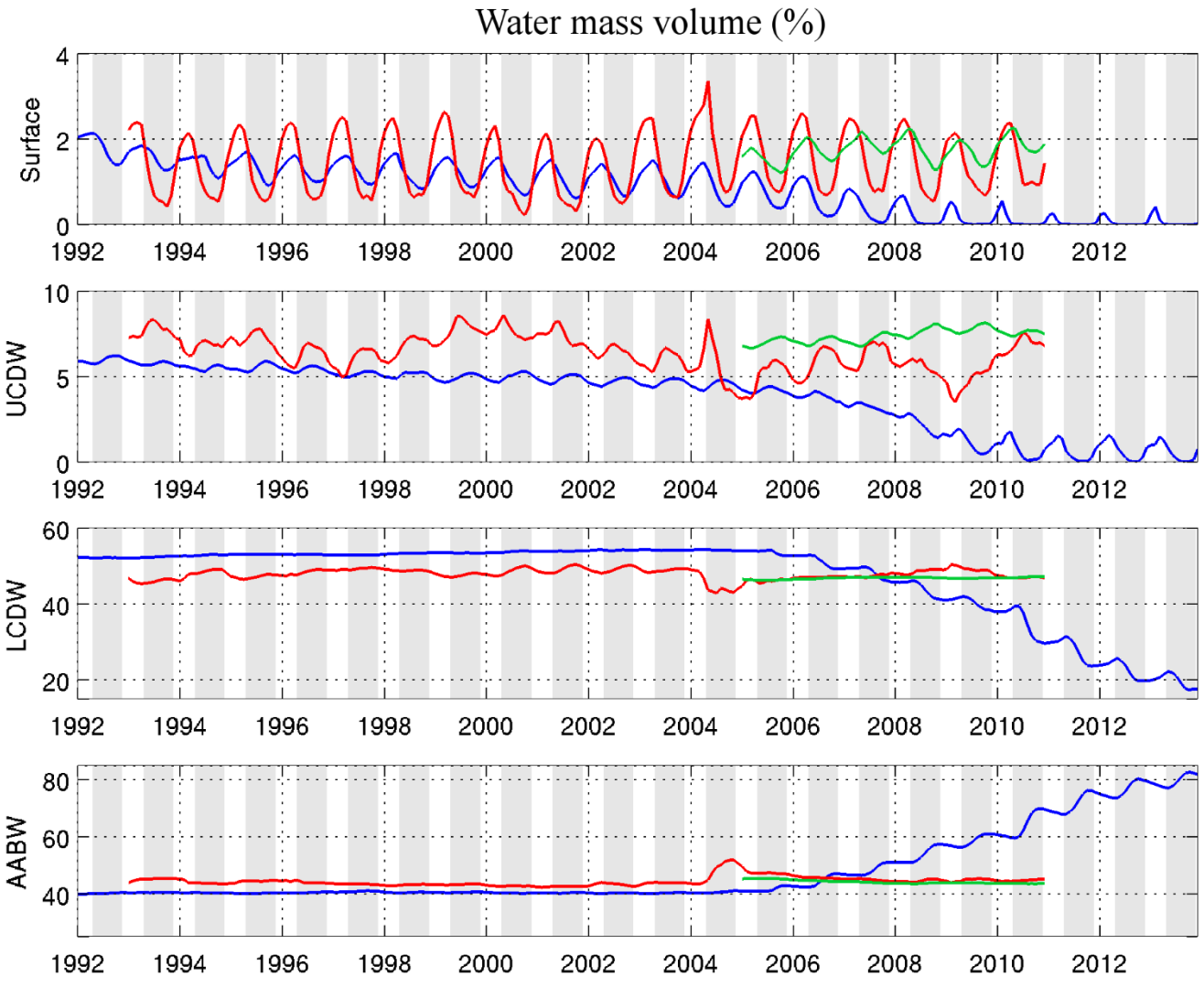

Figure 6: Volume percentage of Indian Ocean sector occupied by the following water mass: *Surface Waters* (γ^n<27.7 kg m^{-3}), *Upper Circumpolar Deep Water* (UCDW; 27.70 kg m^{-3}< γ^n < 28.00 kg m^{-3}), *Lower Circumpolar Deep Water* (LCDW; 28.27 kg m^{-3}< γ^n < 28.00 kg m^{-3}), and *Antarctic Bottom Water* (AABW; γ^n > 28.27 kg m^{-3}). The red, blue, and green lines depict UR025.4, ECCO2, and SoSE reanalysis, respectively

Ocean Sci. Discuss., doi:10.5194/os-2017-9, 2017
Manuscript under review for journal Ocean Sci.
Discussion started: 17 March 2017
© Author(s) 2017. CC-BY 3.0 License.

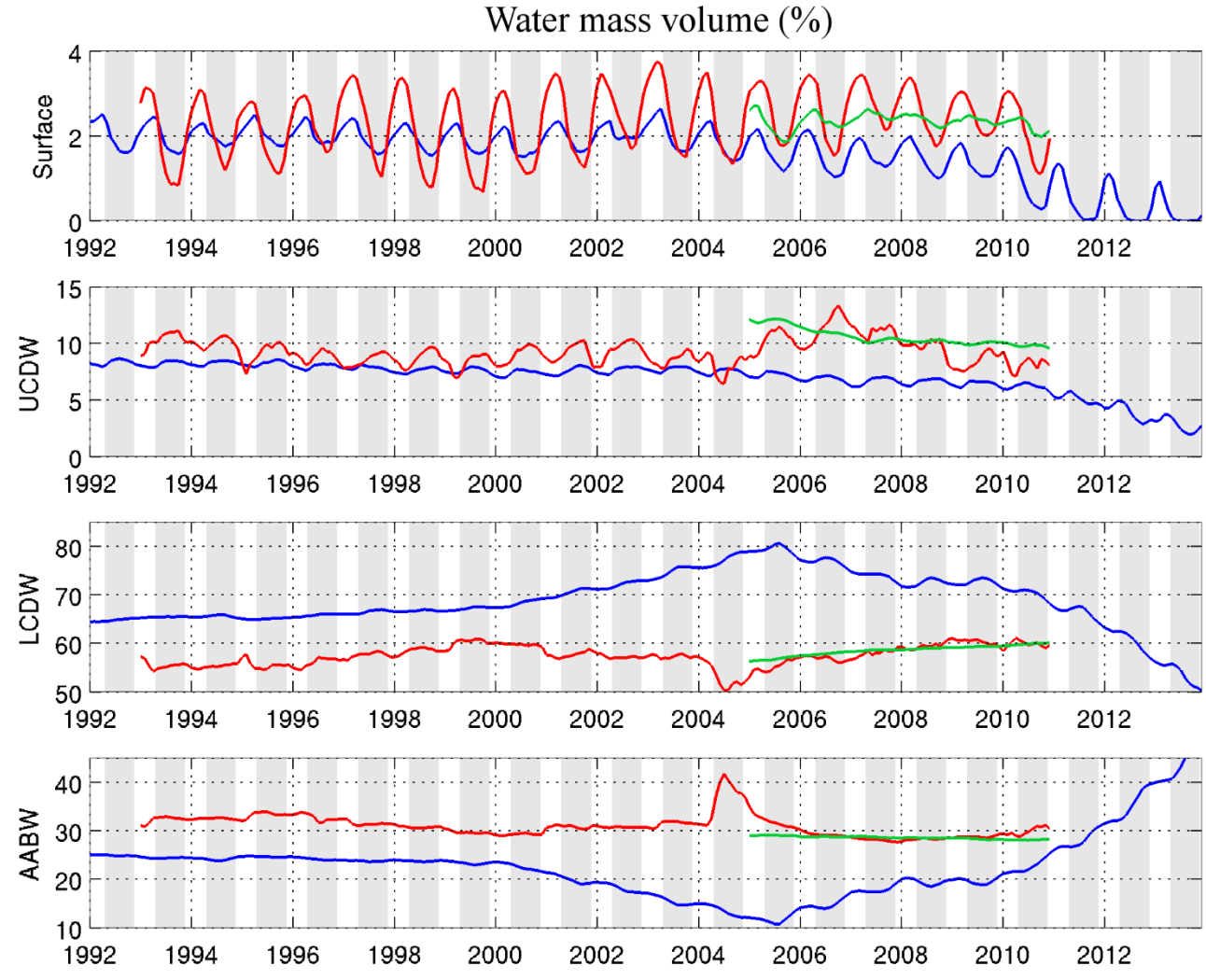

Figure 7: Same as Figure 6, but for the Western Pacific sector.

Ocean Sci. Discuss., doi:10.5194/os-2017-9, 2017
Manuscript under review for journal Ocean Sci.
Discussion started: 17 March 2017
© Author(s) 2017. CC-BY 3.0 License.

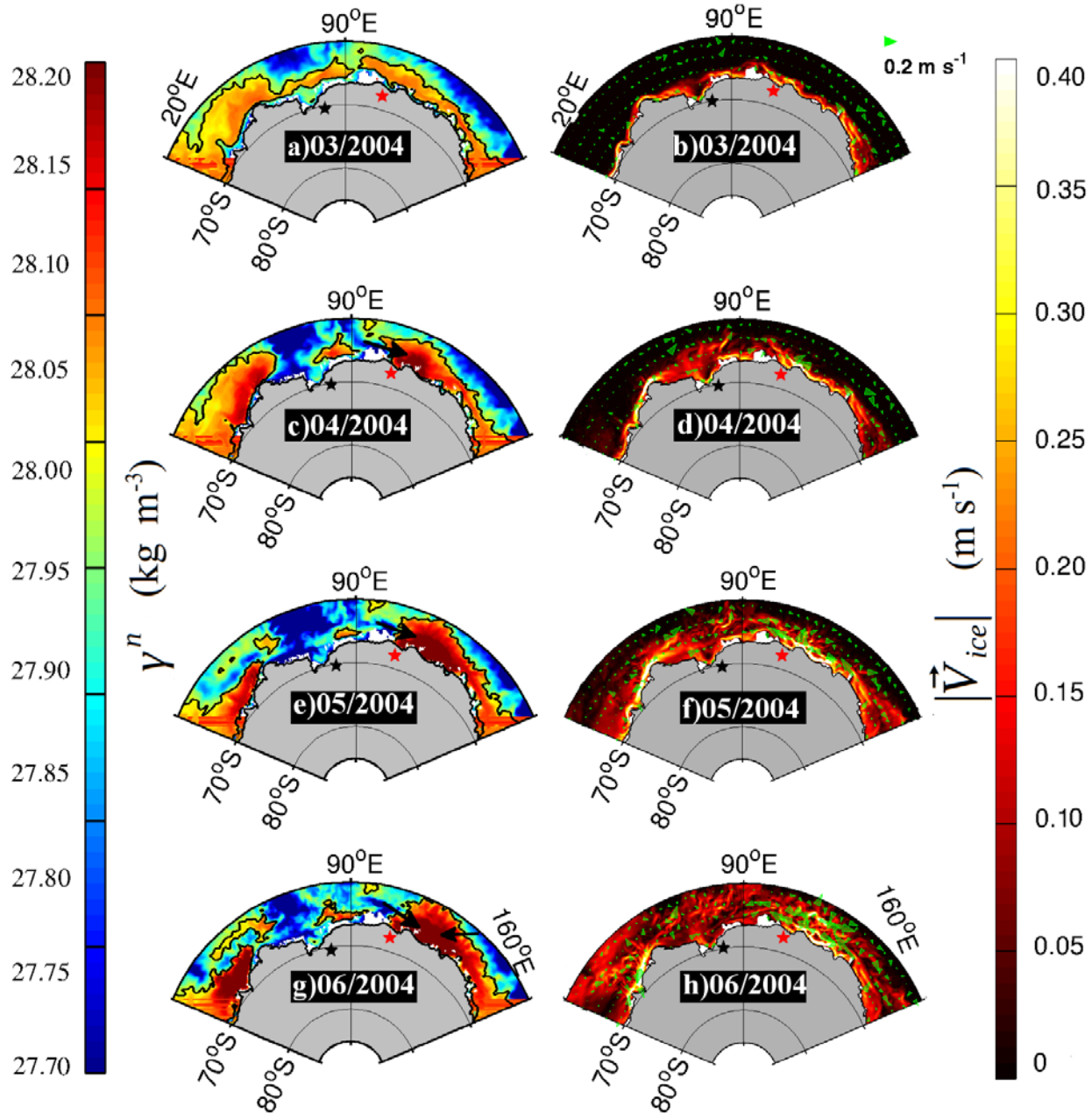

Figure 8: Neutral density distribution at 250 m depth, in the center of the UCDW (27.70 kg m^{-3}< γ^n < 28.00 kg m^{-3}) entrainment, in the Indian Ocean and Western Pacific sectors for (a) March, (c) April, (e) May and (f) June of 2004. The black lines mark the 28.0 kg m^{-3} neutral density surface that distinct the UCDW from LCDW. The black arrow represents the direction of the density gradient. The module of sea ice velocity (m/s) for (a) March, (c) April, (e) May and (f) June of 2004. The green arrows show the ocean current velocity at 250 m. The black (★) and red stars (★) represent the location of Prydz bay and Vincennes Bay, respectively.

Ocean Sci. Discuss., doi:10.5194/os-2017-9, 2017
Manuscript under review for journal Ocean Sci.
Discussion started: 17 March 2017
© Author(s) 2017. CC-BY 3.0 License.

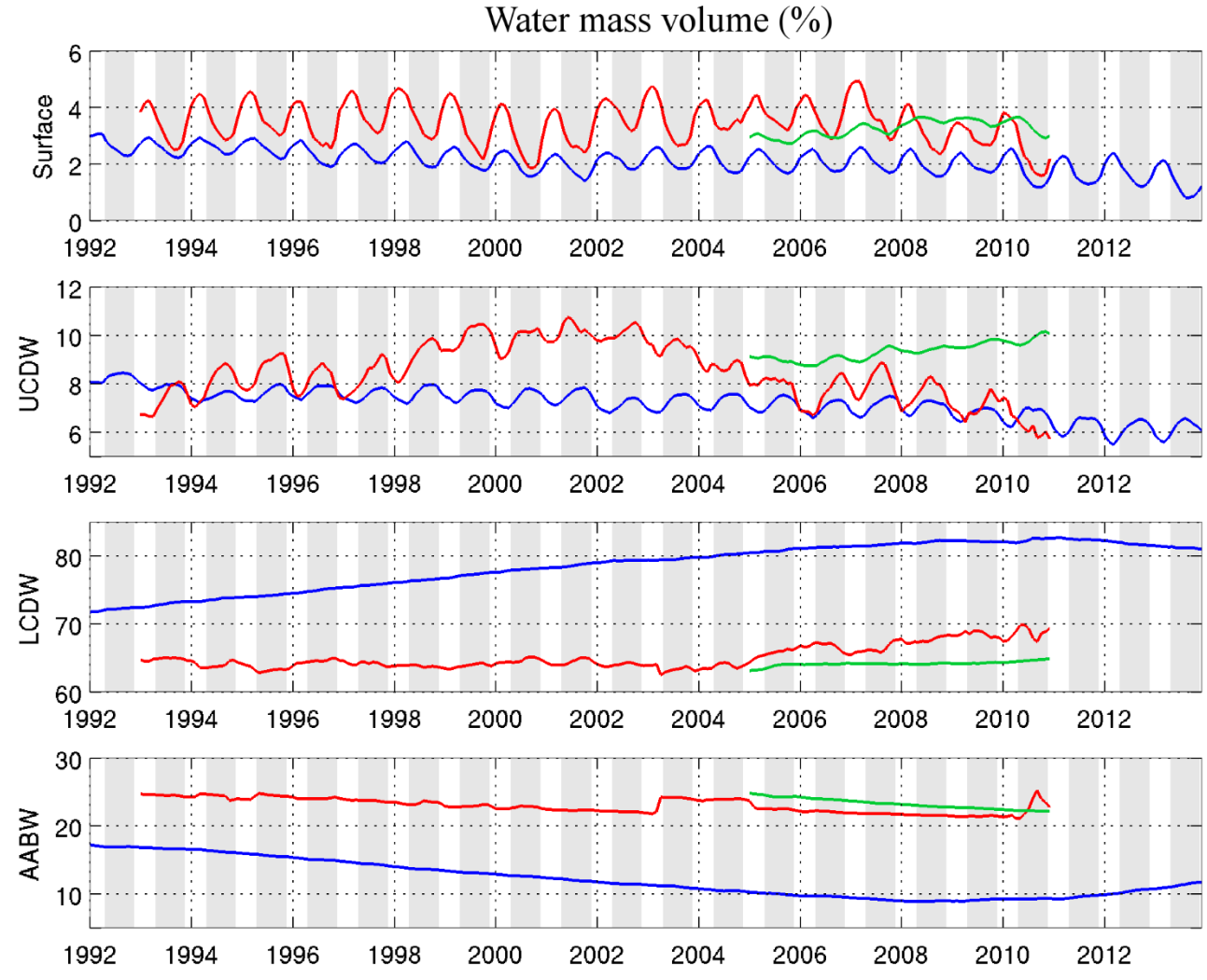

Figure 9: Same as Figure 6, but for the Ross Sea sector.

Ocean Sci. Discuss., doi:10.5194/os-2017-9, 2017
Manuscript under review for journal Ocean Sci.
Discussion started: 17 March 2017
© Author(s) 2017. CC-BY 3.0 License.

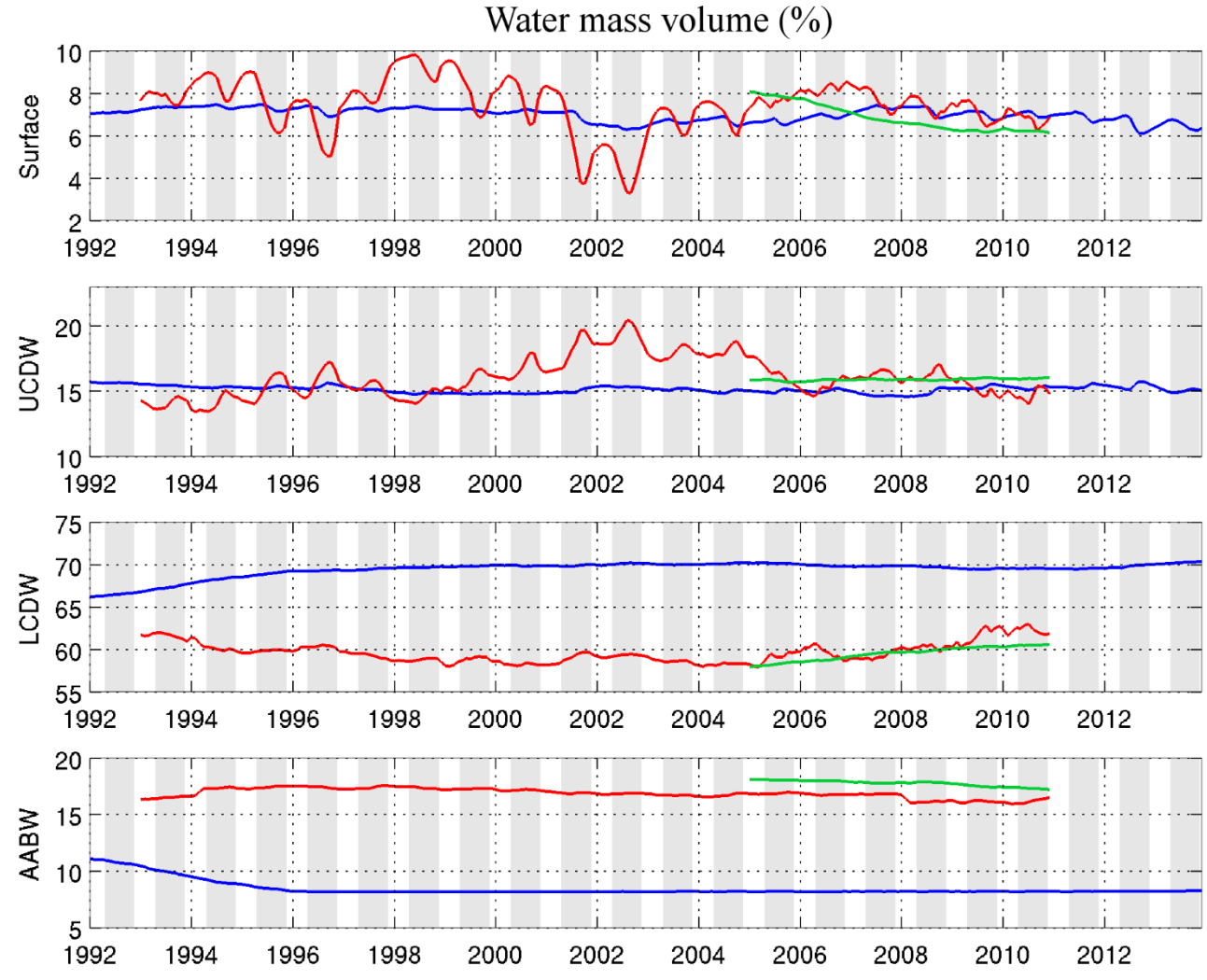

Figure 10: Same as Figure 6, but for the Bellingshausen and Amundsen seas sector.